13

Development of a Human-Friendly Omni-directional Wheelchair with Safety, Comfort and Operability Using a Smart Interface

[1]Kazuhiko Terashima, [2]Juan Urbano, [3]Hideo Kitagawa, and [1]Takanori Miyoshi

[1]*Toyohashi University of Technology*
[2]*Denso Preas*
[3]*Gifu National College of Technology*
Japan

1. Introduction of the OMW

A variety of wheelchairs with different options and special add-on features have been developed to meet a wide range of needs (Pin & Killough, 1994), (Wada & Asada, 1999), (West & Asada, 1992). In order to satisfy the demand for higher mobility, designers have created new driving concepts such as omni-directional movement which allows any combination of forward, sideways, and rotational movement, thus ensuring users much more freedom and safety in wide or narrow spaces.

Autonomous electric wheelchairs are very useful for people who cannot move their upper bodies freely. However, these wheelchairs need to be fitted with a central control unit and high-level sensors capable of realizing complex navigation and obstacle avoidance tasks, based on a description of the environment and final goals marked out by those sensors. Since autonomous wheelchairs can function well only in special environments, this mode greatly limits the user's freedom.

In order to offer users with a higher degree of independence, the user-controlled movement mode, or semi-autonomous mode, which is operated under absolute user control by an input device such as a joystick, switch, monitor, etc., has been developed. The main difference between autonomous and semi-autonomous systems is that in semi-autonomous systems users interact in real time to perform certain tasks in dynamic environments. Under user control, the wheelchair can go wherever the user wants it to. Therefore, this mode provides a high degree of user independence.

However, it is necessary to keep in mind that some elderly people or handicapped people can not use their arms due to weakness or injury. These people need the help of an attendant. In developed countries in which the number of young people is declining yearly, some healthy elderly people are taking care of other elder or handicapped people. For these attendants, a system that helps them to push the wheelchair and its occupant would be very convenient.

Years ago, the main purpose of research was to develop reliable systems without showing great concern for the comfort of the user when employing them. However, with the advent of ergonomics or "the systematic application of knowledge about the psychological, physical, and social attributes of human beings in the design and use of all things which affect a person's working conditions: equipment and machinery, the work environment and layout, the job itself, training and the organization of work", designers have become more aware of the importance of the user when designing any device. Comfort, or "a state of being relaxed and feeling no pain, when using a piece of equipment" emerged as a design goal. This is especially true in the case of wheelchairs where the occupants are weak people because of age or disease.

Therefore, the development of an omni-directional wheelchair that can provides the occupant with semi-autonomous functions and comfort; and the attend with power assist support is highly desirable.

When considering about wheelchairs, it is necessary to remember that they can be classified in two main groups: manual wheelchairs or wheelchairs that move due to the application of force by the occupant, and electric wheelchairs, or wheelchairs that employ electric energy for generating movement. Just the latter are the object of interest for this research.

In order to offer users with a higher degree of independence, the user-controlled movement mode, or semi-autonomous mode, which is operated under absolute control of users by an input device such as joystick, switch, monitor, etc., has been developed. Under control of users, wheelchair can go wherever users want to go. Therefore, this mode provides a great independence to users. For achieving reliable navigation, obstacle detection and collision avoidance must be considered when designing a wheelchair. In the case of semi-autonomous wheelchairs, most of them rely on reactive obstacle avoidance (Argyros et al., 2002), (Borgolte et al., 1998), (Levine et al., 1999), (Tahboub, 2001), (Yanco et al., 1995) which is in some degree safe but uncomfortable for the user if he is not aware of the obstacle and he is unexpectedly taken away from it. "Not being aware" means that the user is not giving attention to the environment or maybe he is a blind one. It means that environment information must be provided in a way that it can be perceived without using the eyes. Most of semi-autonomous wheelchairs use joysticks as input devices then it appears natural to provide environment information to users through joystick. That is, joystick becomes a haptic device, or a device that provides information through the sensation of touch.

Many power-assisted wheelchairs have been developed for handicapped people who have free use of their arms. Power assist is useful for reducing the burden of manual workers and elderly people. In recent years, it is necessary for elderly people to support other elderly people. Research on power-assist systems has been widely reported (Hayashibara et al., 1999), (Kawai et al., 2004), (Kumar et al., 1997), (Lee et al., 1999), (Naruse et al., 2005) and much study has been devoted to wheelchairs (Sanada et al., 2005), (Seki et al., 2005), (Wu et al., 2004) regarding the chair's straight-line forward and backward movement. However, in spite of its importance, little study has focused on power-assist with respect to rotation, lateral and slanting movements. The application of power-assist for supporting the attendant of an omni-directional wheelchair constitutes a new area of research. Though some research regarding a power-assist system for omni-directional vehicles related to carts is available (Maeda et al., 2000), no report regarding this topic as related to wheelchairs has appeared, to the authors' knowledge. In the case of the Omni-directional Cart with Power-assist System developed by Matsushita Electric Works (Maeda et al., 2000) a cart with the

length being bigger than the width is considered. In this case, they report problems with lateral motion when the length of the cart is very big. Moreover, it looks like they have considered turning, but not rotation over the center of gravity because it could not be possible due to the dimensions of the cart. On the other hand, achieving almost perfect rotation over the center of gravity and high accuracy in lateral and forward-backwards motion is a very important goal in this research.

In recent years special attention has been given to ride comfort. When ride comfort is studied, most of them consider only influences of vibration in up-down direction caused by uneveness of the ground. Various alternatives have been mooted to solve this problem, however, most of them are based on more or less complex mechanical solutions such as soft cushions, vibration absorber, etc. (Sato et al., 2003). With the use of these advanced equipments, the cost has been increased accordingly and, moreover, it also usually increases the weight of the device. According to literature, when automobile drivers were asked about parameters necessary to driving comfort, they mentioned factors such as a well designed seat, adjustable features, correct temperature, ease of reaching controls and pedals, enough space, low noise level as well as vibration-free riding.

For wheelchair users, the factors related to comfort are almost the same as those mentioned above. In fact, two main problems are considered when designing a comfortable wheelchair: comfortable seat design and suppression of vertical vibration caused by rough pavement or the wheelchair's mechanical elements. However, there is another factor that must be considered: vibration due to jerking, or the variation of linear acceleration (Seki et al., 2005). When the natural frequency of this vibration synchronizes with the natural vibration frequency of human beings, the resonance phenomenon causes large oscillations and therefore leads to the discomfort of the wheelchair's occupant. In past studies (Matsuoka, 2000a), (Matsuoka, 2000b), (Nishiyama, 1993), (Okada, 1980), (Smith, 2000), the user's upper body is considered as a series of rigid segments (head, chest, waist) connected by flexible joints. Each joint is given a rotational spring constant (RSC) and a rotational viscous damping constant (RVDC). However, since waist is connected to the seat directly, its swing frequency is much less than that of head and chest. Then, in this research, in order to simplify the model, it is considered that upper human body consists of two rigid segments: head and torso. Moreover, in this research the human model is used for studying vibration of the human body when it moves in a horizontal plane, while previous researchers have used a human model for studying the problem of vibration of the human body when it moves in a vertical direction.

In author's laboratory, a holonomic Omni-directional Wheelchair (OMW) which can act as an autonomous (Kitagawa, Terashima et al., 2002), semi-autonomous (Kitagawa, Terashima et al., 2001) or power assisted (Kitagawa, Terashima et al., 2004) wheelchair has been developed. Because of its omni-directional movement, it is able to navigate smoothly in structured inner environments using range sensors for getting environment information. In order to recognize surrounded environment it can build a local map which provides distance to nearest obstacles. In semi-autonomous mode the input device is a joystick, with velocity of OMW being proportional to the angular displacement of the joystick. In previous research, just the idea of haptic feedback was proposed (Tahboub, 2001), or a combination of a haptic joystick with a virtual simulator for navigation was used (Protho et al., 2000). In this research, a wheelchair provided with a haptic joystick has been built. Moreover impedance of joystick or force feedback changes according not only to velocity of OMW but also to the

distance of OMW to the nearest obstacle in the direction of movement. The nearest the distance becomes, the more difficult it becomes to move the joystick, then the user understands that he is going to collide against an obstacle soon an he can decide to change the direction of movement or to stop OMW. The proposed approach by haptic joystick has been tested with good results (Kitagawa , Terashima et al., 2001) , and furthermore, a novel navigation guidance system to induce evasive movement, while the omni-directional wheelchair performs slide movement without rotated movement, using the haptic feedback joystic is proposed.. The obstacle existing toward the moving direction of vehicle has possibility of collision. Therefore, when the obstacle exists in the direction of the OMW's movement, this approach gives the joystick force to operator's hand such that induces evasive movement to navigate OMW toward the direction without obstacle for operator's safe and smooth driving. The purpose of this study gives a support system to realize operator's safe and smooth driving when the operator passes through the narrow aisle, entrance of room, or enters an elevator,etc.(Kondo, et al. 2008).

In the power assisted mode, in the authors' laboratory (Kitagawa, Terashima et al., 2004) a six-axis force sensor is used for measuring the force applied by the attendant in two orthogonal axes, X and Y, and a rotational direction θ. This force is then changed to reference velocity V_x, V_y, and ω by using a first-order lag controller. Finally, the reference velocity is applied to the servo-motors of the OMW. This system works well as a power-assist system, and provides the attendant effective support. However, a problem related to the operability of the OMW remains. Due to the application of the power-assist system, the operability of the OMW diminishes especially when the attendant tries to rotate the chair in a clockwise (CW), or counter-clockwise (CCW) direction around the OMW's center of gravity CG.

A survey was conducted among various attendants trying to discover some relationships in the way they developed forwards-backwards, lateral, and rotational movements. It was impossible to find general rules that explained all cases, but a relationship was found between lateral and rotational movements. These relationships were used as the basis for constructing a fuzzy reasoning system (Mathworks, 2002), (Harris et al., 1993), (Mamdani & Assilian, 1985), (Shaw, 1998), (Sugeno & Kang, 1998), (Takagi & Sugeno, 1985) that helped to improve the operability of the OMW. An expert operator can move the OMW with ease, but for people not accustomed to its use it is difficult to easily manage in any direction. Thus, the development of a novel power-assist system with easy operability is strongly demanded. In this paper, this system is called a "skill-assist system" (Yamada et al., 2002).

Nevertheless, when the system was tested by different attendants, a completely satisfactory result was not obtained by every attendant, since each operator has his or her own tendencies, and thus the parameters of the fuzzy inference system must be reasonably tuned to respond to the individual. Tuning the fuzzy inference system by trial and error was thus attempted and its results reported in (Kitagawa, Terashima et al., 2004). This was found to be a time-consuming process, leading to fatigue and boredom in the attendants.

Hence, a better tuning method, a method that allows tuning of the fuzzy inference system, is needed. This can be obtained by adding Neural Networks (NN) to the fuzzy inference system, obtaining what is known as a neuro-fuzzy system. Much research has been devoted to this topic (Jang, 1993), (Jang et al., 1997), (Juang & Lin, 1998), (Lian et al., 1999), (Lin & Lee, 1991), (Nguyen et al., 2003). Jang (Jang, 1993) developed the ANFIS (Adaptive-Network-based Fuzzy Inference System), a neuro-fuzzy system in which the fuzzy inference

system is tuned by using the system's input data. Tuning is performed by minimizing the output error of the NN used in combination with the fuzzy inference system. For achieving this goal, the NN is trained by using a hybrid method that combines least squares and the Backpropagation algorithm (BP law). This method is thus thought to be an effective method for tuning the parameters of the OMW's fuzzy inference system.
In the case of comfortable navigation, in the authors' laboratory comfort has been a subject of study in the autonomous mode without the joystick (Terashima et al., 2004) but only when the OMW moves in a single direction, X or Y. In the present paper, comfort is studied when the OMW moves in any direction, such as a slanting direction, when in practical semi-autonomous operation mode using the joystick (Urbano et al., 2005b). For the command input via joystick operation, the velocity control of the OMW is carried out by means of frequency shaping using the Hybrid Shape Approach (HSA) proposed by the authors (Yano et al., 2000) in order to achieve the swing suppression control or comfortable driving by excluding a specific spectrum of elements such as the natural frequency of the OMW and the discomfort frequency of human organs. A human model which considers the human upper body to be composed of two parts, the torso and head, has been developed and used in order to test the effectiveness of the proposed approach.

In this chapter, in section 2, kinematics and dynamics of the OMW are described. In section 3, semi-autonomous operation and guidance system of the OMW for obstacle avoidance by haptic joystick. In section 4, power asist control of OMW for helper and, in section 5, adaptive control by Neuro-Fuzzy system of OMW using a touch Panel as human interface for realizing tailor-made vehicle. In section 6,comfort driving of the OMW and conclusion in section 7.

2. Kinematics and dynamics of the OMW

The OMW, which can act as an autonomous (Kitagawa et al., 2002), semi-autonomous (Kitagawa et al., 2001) or power assisted (Kitagawa et al., 2004) wheelchair is shown in Fig. 1, and its specifications are shown in Table 1.

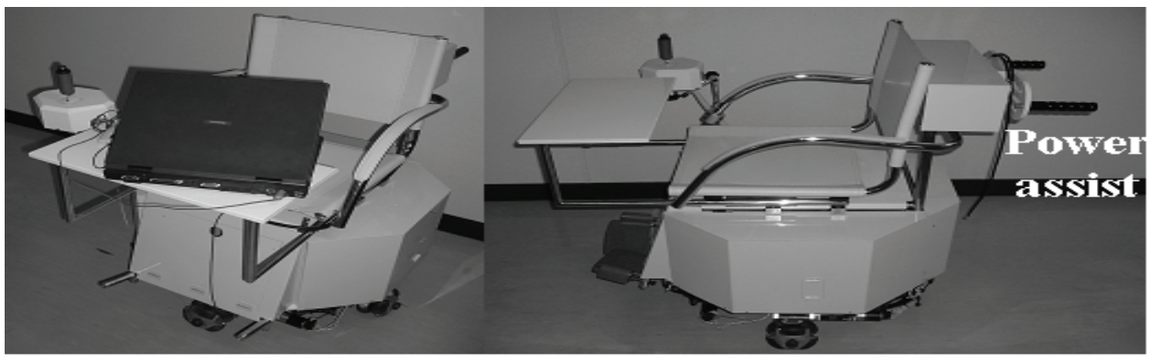

Fig. 1. Omni-directional wheelchair (OMW)

The OMW is able to move in any arbitrary direction without changing the direction of its omni-wheels, which are shown in Fig. 2. In this system, four omni-directional wheels are

individually driven by four motors, as shown in Fig. 3. Each wheel has passively driven free rollers at its circumference. The wheel that rolls perpendicularly to the direction of movement does not stop its movement, because of the passively driven free rollers. These wheels thus allow movement that is holonomic and omni-directional.

Size	Width	0.70 [m]
	Depth	1.50 [m]
	Height	1.10 [m]
Weight		70 [kg]
Maximum velocity		1.0 [m/s]
Maximum accelaration		0.5 [m/s^2]

Table 1. Specifications of the OMW

Fig. 2. Omni-wheel

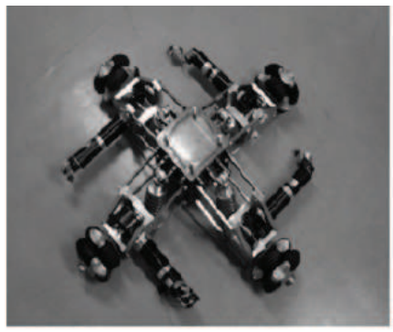

Fig. 3.Omni-wheels and motors

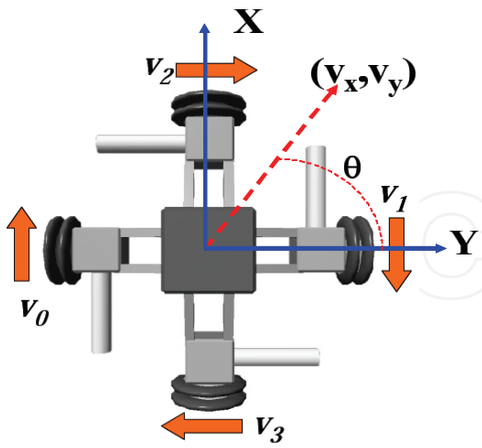

Fig. 4. Velocity vectors of the omni-wheels

In the coordinate system of the OMW, the X-axis is defined when the OMW moves forward or backward. The Y-axis is defined when the OMW moves to the right or left, and rotational

direction is defined according to direction θ perpendicular to the plane determined by X and Y. The joystick's coordinate system is established in the same way as that of the OMW. Furthermore, if V_x is the velocity of the OMW in the X-axis, V_y the velocity of the OMW in the Y-axis, and ω the angular velocity of the OMW when it rotates around the vertical axis, the velocity of the OMW can be expressed as $V_{OMW} = [V_x, V_y, \omega]^T$. The velocity of the OMW is the vectorial sum of the velocities of the four omni-directional wheels. The velocity vector for the omni-wheels is written as $V_{WHEEL}= [V_0, V_1, V_2, V_3]^T$. The velocity vectors corresponding to each omni-wheel are shown in Fig. 1. In Fig. 4, θ is the angle that the velocity vector of the OMW has with the axis Y of the reference system.

From Fig. 4:

$$V_x = \frac{1}{2}(V_0 - V_1) \tag{1}$$

$$V_y = \frac{1}{2}(V_2 - V_3) \tag{2}$$

$$\omega = \frac{1}{4l_{\omega b}}(-V_0 - V_1 - V_2 - V_3) \tag{3}$$

, where $l_{\omega b}$ is the distance from the center of the OMW to the circumference of the omni-wheels. Written in a matrix form, the above equations become:

$$V_{OMW} = B \cdot V_{WHEEL} \tag{4}$$

where

$$B \equiv \begin{bmatrix} \frac{1}{2} & -\frac{1}{2} & 0 & 0 \\ 0 & 0 & \frac{1}{2} & -\frac{1}{2} \\ -\frac{1}{4l_{\omega b}} & -\frac{1}{4l_{\omega b}} & -\frac{1}{4l_{\omega b}} & -\frac{1}{4l_{\omega b}} \end{bmatrix} \tag{5}$$

Since generally a matrix should be square in order to calculate its inverse, the coefficients' matrix in Eq. (4) should be square in order to calculate V_{WHEEL} from V_{OMW}. Keeping this in mind, the angular velocity ω of OMW is divided into two parts: ω_1 produced by V_0 and V_1, and ω_2 produced by V_2 and V_3.

$$\omega_1 = \frac{1}{2l_{\omega b}}(-V_0 - V_1) \tag{6}$$

$$\omega_2 = \frac{1}{2l_{\omega b}}(-V_2 - V_3) \tag{7}$$

$$\omega = \frac{1}{2}(\omega_1 + \omega_2) \tag{8}$$

By using Eq. (6), Eq. (7) and Eq. (8), it is possible to get:

$$\begin{bmatrix} V_x \\ V_y \\ \omega_1 \\ \omega_2 \end{bmatrix} = \begin{bmatrix} \frac{1}{2} & -\frac{1}{2} & 0 & 0 \\ 0 & 0 & \frac{1}{2} & -\frac{1}{2} \\ -\frac{1}{2l_{\omega b}} & -\frac{1}{2l_{\omega b}} & 0 & 0 \\ 0 & 0 & -\frac{1}{2l_{\omega b}} & -\frac{1}{2l_{\omega b}} \end{bmatrix} \begin{bmatrix} V_0 \\ V_1 \\ V_2 \\ V_3 \end{bmatrix} \tag{9}$$

V_{OMW} can be expressed by:

$$\begin{bmatrix} V_x \\ V_y \\ \omega \end{bmatrix} = \begin{bmatrix} 1 & 0 & 0 & 0 \\ 0 & 1 & 0 & 0 \\ 0 & 0 & \frac{1}{2} & \frac{1}{2} \end{bmatrix} \begin{bmatrix} V_x \\ V_y \\ \omega_1 \\ \omega_2 \end{bmatrix} \tag{10}$$

For avoiding the slippage of the wheels, the constraint $\omega_1 = \omega_2$, or $V_0 + V_1 = V_2 + V_3$ is imposed. By considering $\omega_1 = \omega_2$, Eq. (9) can be expressed as follows:

$$V_{WHEEL} = B^{*-1} \cdot V_{OMW} \quad , \tag{11}$$

, where

$$B^{*-1} \equiv \begin{bmatrix} 1 & 0 & -l_{\omega b} \\ -1 & 0 & -l_{\omega b} \\ 0 & 1 & -l_{\omega b} \\ 0 & -1 & -l_{\omega b} \end{bmatrix} \tag{12}$$

Here, $\mathbf{B}^{*-1}$ is a pseudo-inverse matrix that allows the velocity of each wheel to be obtained based on the velocity of the OMW.

3. Semi-autonomous Operation and Guidance System of the OMW for Obstacle Avoidance by Haptic Joystick.

The OMW is able to move in any arbitrary direction without changing the direction of the wheels. In this system, four omni-directional wheels are individually driven by four motors.

Each wheel has passively driven free rollers at its circumference. The wheel that rolls perpendicularly to the direction of movement does not stop its movement because of the passively driven free rollers. Thus, these wheels allow holonomic and omni-directional movement.

The obstacle detection sensors are activated in back and forth of the OMW in order to obtain information regarding its surrouding environment. In this research, the input device is a joystick. The direction of the vehicle movement depends on orientation of the joystick and speed is proportional to declination of the joystick. Moreover, two motors are installed in each x and y axis of the joystick, and the joystick can give virtual spring damper characteristics because of the impedance control. (Kitagawa et al, 2001), (Urbano et al, 2005a).

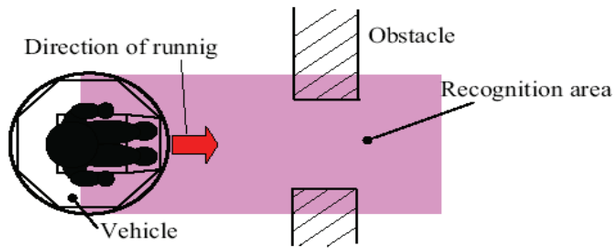

Fig. 5. Schematic diagram of environmental recognition and navigation

It is possible to acquire the surrounding environmental information in real time by two obstacle detection sensors. The obstacle with danger collision exists in the direction of OMW's running with current input. Therefore, the algorithm that choses only environmental information which exists in the direction of the OMW's running from all of the obtained information is constructed. Figure 5 shows the otuline of the environmental recognition system. The recognition area can be changed, corresponding to the direction of OMW's running.

Detection range	20~4000 mm
Accuracy	± 10 mm
Angle range	240°
Angular resolution	0.36°
Response time	100 ms

Fig. 6. Specification of obstacle detection sensor

The specifications of the obstacle detection sensor "URG-04LX" (Hokuyo Automatic Co. Ltd.) are shown in Fig. 6. This sensor gives real-time updates of the surrounding environment. The sensor covers a wide angular range. The maximum angular resolution on

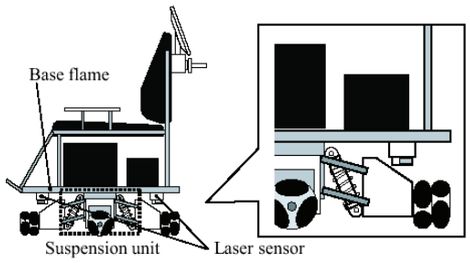

Fig. 7. Configuration of obstacle detection sensor (1)

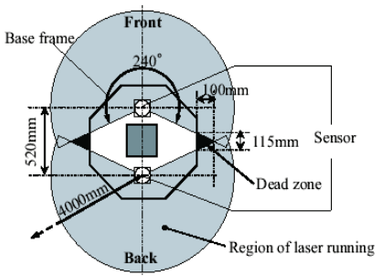

Fig. 8. Configuration of obstacle detection sensor (2)

the sensor is 0.36 [deg] within range of 240 [deg]. And measurement range of the sensor is 20-4000 [mm]. Furthermore, it only takes 100 [ms] for one complete scan. In this research, the angular resolution is applied 3.6 [deg] for the brevity of calculations. Two sensors are attached on frontside and backside of the base frame, where the control unit, the chair and the battery is installed, as shown in Fig. 7. It is possible to get the surrounding environmental information without shelding matters, because the unit above the base frame is braced with the suspension unit at the OMW's center, as shown in Fig. 4. Then, there are small dead areas in laser sensors' scanning in OMW's right and left sides, as shown in triangle black zone in Fig. 8. These dead areas are regarded as a part of OMW as described later. The total output response time to capture environmental map is 200 [ms] in this system, because of using two obstacle detection sensors. Take into account of the velocity of OMW's movement and velocity response of OMW, the response time is of no matter.

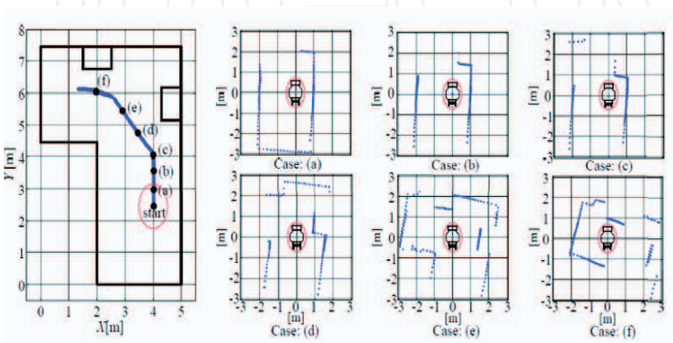

Fig. 9. Experimental result of obtaining environmental information

Figure 9 shows experimental results of obtaining environmental information using the obstacle detection sensor, while human operates the joystick for navigation. In this experiments, the OMW is manually controlled using joystick by operator. Note that, the obstacle and wall is recognized as points, and the map described by points is rotated while OMW is skew movement. It should be considered that this phenomenon is caused by slipping of the omni-wheel ad differences in the diameter of each four omni-wheels.
In this section, the algorithm that choses only environmental information existing toward the moving direction of the OMW from all the surrounding environmental information is presented.

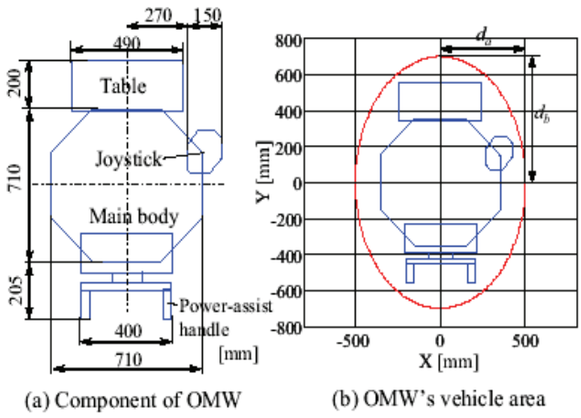

(a) Component of OMW (b) OMW's vehicle area

Fig. 10. Definition of OMW's vehicle area

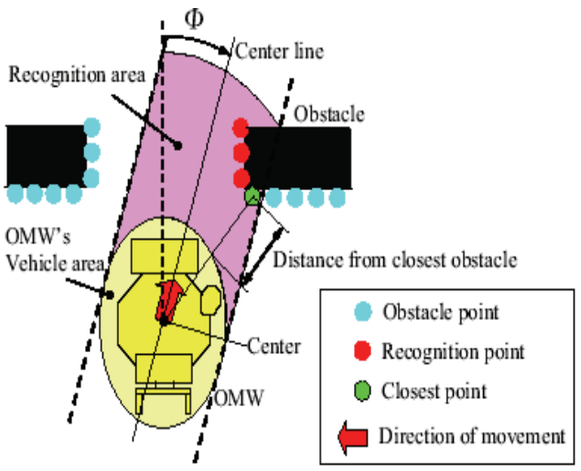

Fig. 11 . The environmental recognition system

First, the OMW's vehicle area which covers the entire OMW is defined. Since the OMW has a table, the joystick, and the power-assist handle, the OMW's vehicle area is defined as the shape of an ellipse covering both parts of OMW's main body and the dead areas of laser scanning as shown in Fig. 7(a). The length of shorter axis of this ellipse is d_a = 0.5 [m] and

longer axis is d_b = 0.7 [m], as shown in Fig. 7. If the obstacle goes inside the OMW's vehicle area, it is considered as a crashing obstacle. Next, an algorithm such that only environmental information existing toward the moving direction of the OMW is chosen, is proposed. Now the OMW is slide moving in direction Φ, as shown in Fig. 11. Then the surrounding environmental information is acquired as a set of points by two obstacle detection sensor. These points set are defined as the obstacle points. The straight line drawn by extending the moving direction from the OMW's center point is defined as the center line. The area between two lines such as being parallel to the center line and tangent to the oval vehicle area, is defined as the recognition area. And the obstacle points existing in the recognition area are defined as the recognition points, The closest recognition point to the OMW's vehicle area is defined as the closest point. Thus, the obstacle existing in the recognition area has danger of collision with OMW. By means of this algorithm, the present system can recognize only the obstacle with possibility of collision of the present moving direction, and teach the distance to the closest recognition point to the OMW. And the environmental recognition system achieves high speed response time to capture environmental map, compared with velocity response of OMW. Therefore, if navigator suddenly changes the joystick's direction, navigator's safe is assured with the presented system.

Derivation of the recognition area is explained in more detail. Now, the vehicle is moving in the direction Φ. A perfect circle shape is defined as the vehicle area. In this algorithm, the vehicle area needs to be perfect circle, but the OMW's vehicle area is really ellipse shape. Therefore, in order to change the shape of OMW's vehicle area into a perfect circle shape, the scale of X-axis or Y-axis is temporarily altered while picking the recognition point. For example, in this study case, all of Y-coordinate value of obstacle points times d_a/d_b, because the OMW's vehicle area is defined as shape of an ellipse, and the length of shorter axis is d_a = 500 [mm] on the X-axis and longer axis is d_b = 700 [mm] on the Y-axis, as shown in Figure 7. And movement direction Φ is converted into Φ′ by following equation (dash ″, ″ indicates the transformed scale of X-Y axis).

$$\Phi' = \tan^{-1}\left(\frac{\sin \Phi}{d_a / d_b \cdot \cos \Phi} \right) \tag{13}$$

First, the circumstance of the vehicle is divided into the layer of l thick ($L1;L2;\ldots;Ln$) and the obstacle points are stored in these layer. Next, the range of angular is derived in several layers such as

$$\Phi' - \theta'_n \le \Theta'_n \le \Phi' + \theta'_n, \quad (n = 1,2,3 \ldots n) \tag{14}$$

$$\theta'_n = \sin^{-1}\left(\frac{r + nl}{r} \right) \tag{15}$$

The range of angular Θ_n' is indicated the range of the recognition area on n^{th} layer. If the obstacle point exists in the recognition area, this point is defined as the recognition point.

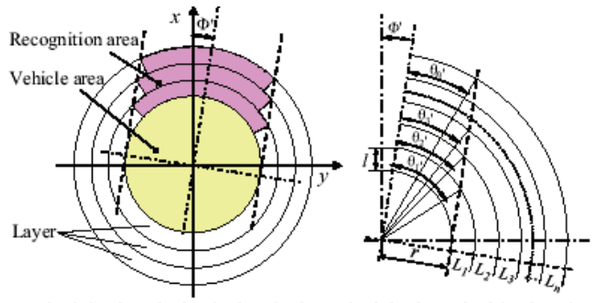

Fig. 12. Definition of recognition area

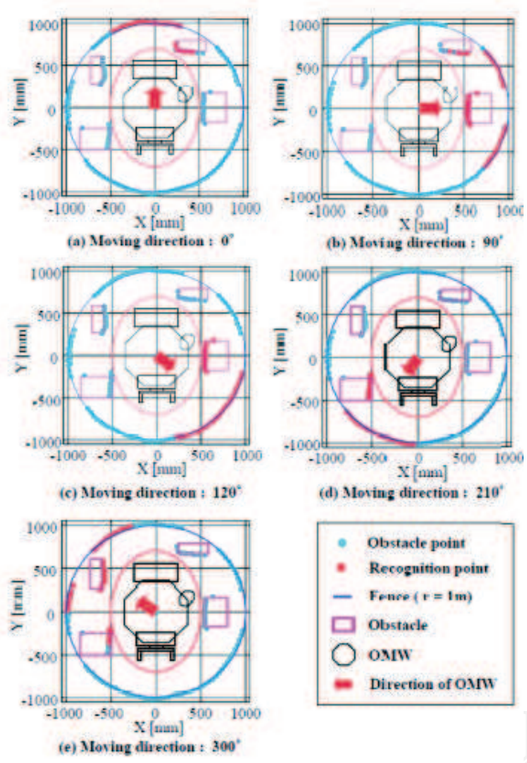

Fig. 13. Experimental results of environment recognition system

After picking the recognition points from all of the obstacle point with the use of above algorithm, all of the Y-coordinate value of obstacle points and recognition points times d_b/d_a in order to reconvert the transformed scale of X-Y axis. The experiment of the environmental recognition system with the recognition area is conducted. The OMW is installed at the center of the fence of radius 1 [m], and four obstacles are installed between the OMW and the fence. The fence is made of white board. The result of this experiment is shown in figure 10. Then, the thickness of the layers is l = 50 [mm]. Note that, the width of the recognition area is changed to fit the OMW's vehicle area defined as shape of an ellipse, and this system can pick out the recognition points from the obstacle points.

Two motors are installed in each x and y axis of the joystick as shown in Fig. 14, and the joystick can give virtual spring-damper characteristics with the impedance control. Based on the distance to the closest obstacle and the wheelchair's input velocity, the impedance of the joystick is provided. By neglecting the effect of joint mechanical compliance and link flexibility, the desired elastic behavior can be described as

$$\tau = d\dot{q} - kq \tag{16}$$

where τ is the joystick's motor torque, d is viscous damping coefficient, k is the stiffness and q is the tilting angle from the neutral position. The viscous damping coefficient is d = 0.015. The desired stiffness k in the input direction of the joystick is described as the following equation, as explained in (Kitagawa et al, 2001).

$$k = k_0 \left\{ \frac{v / v_{\max} + \alpha}{(r / r_{\max})^2} + 1 \right\} \tag{17}$$

where v is the input velocity of the wheelchair, and r is the distance to the nearest obstacle in the input direction. The maximum input velocity is v_{max} = 1.0 [m/s], and the maximum distance in effectiveness range for this impedance control is r_{max}=3.0[m]. The standard stiffness is k_0 = 0.5 [Nm/rad], and the constant value is α= 0.014, determined considering the operator's characteristics of handling etc., as explained in (Kitagawa et al, 2001). The input direction is measured by potentiometers attached to the joystick, as shown in Fig. 15, and the distance to the nearest obstacle r is given by the environmental recognition system described above (Fig. 12).

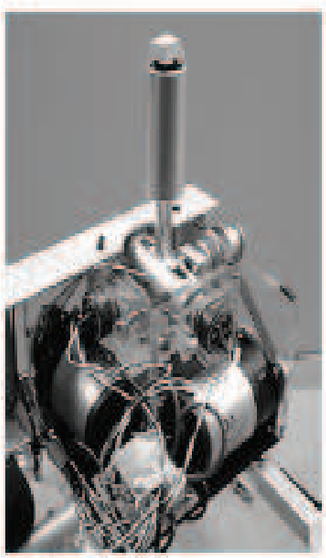

Fig. 14. Joystick

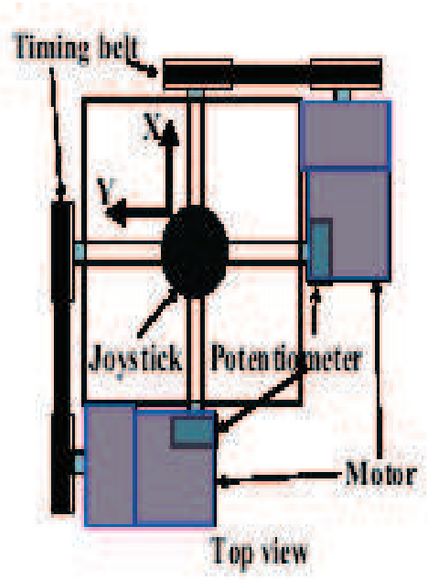

Fig. 15. Joystick system

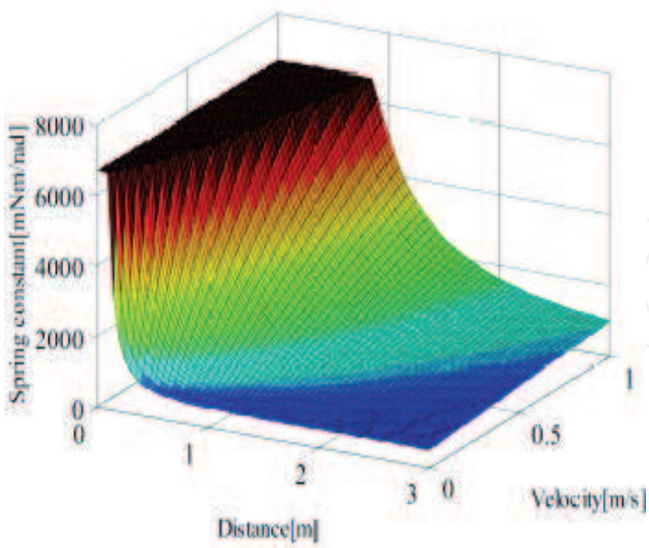

Fig. 16. Plots of stiffness against distance and velocity

Figure 16 shows plots of stiffness k against the distance r and the velocity v in the corresponding direction. Note that, as the distance r becomes smaller, the stiffness k becomes larger, moreover, as the velocity v becomes larger, the stiffness k becomes larger. In the case that the velocity is high, the motion is highly restricted, for safety. In the case that the velocity is low, the motion is scarcely restricted for maneuverability. The operator's input torque is restricted by the impedance of the joystick, hence the motion of the wheelchair is also restricted by means of the operator's joystick commands. Then, given the joystick's motor torque τ by this impedance control system is generated in the opposite direction from the declined direction of joystick by the operator.

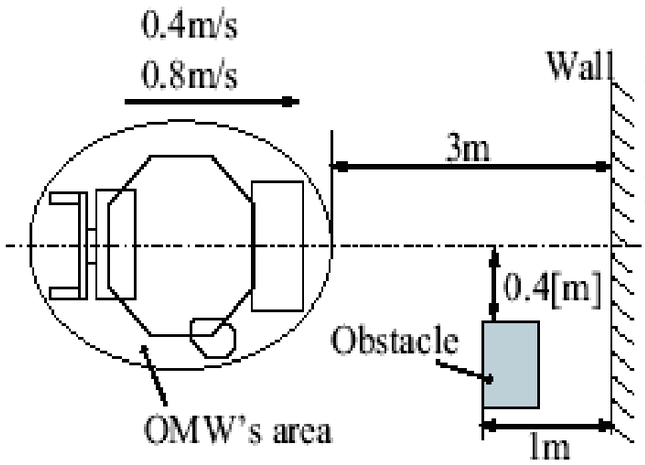

Fig. 17. Experimental condition of impedance control by using joystick

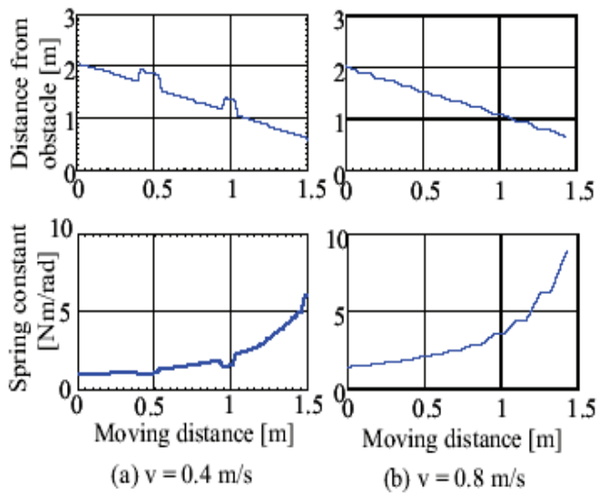

Fig. 18. Experimental result of impedance control by using joystick

Figure 18 shows an experimental result through environmental feedback using obstacle detection sensors while human operates the joystick for navigation. The stiffness k is inspected while the OMW advances toward the wall 3 [m] away from the OMW at a controlled velocity, as shown in Fig. 17. Then, the obstacle is installed between the OMW and wall. Note that, the stiffness k increases as the distance to the obstacle becomes smaller, hence the motor torque grows. Next, the stiffness k is calculated corresponding the direction of joystick's declination, using experimental result shown in Fig. 9, above.

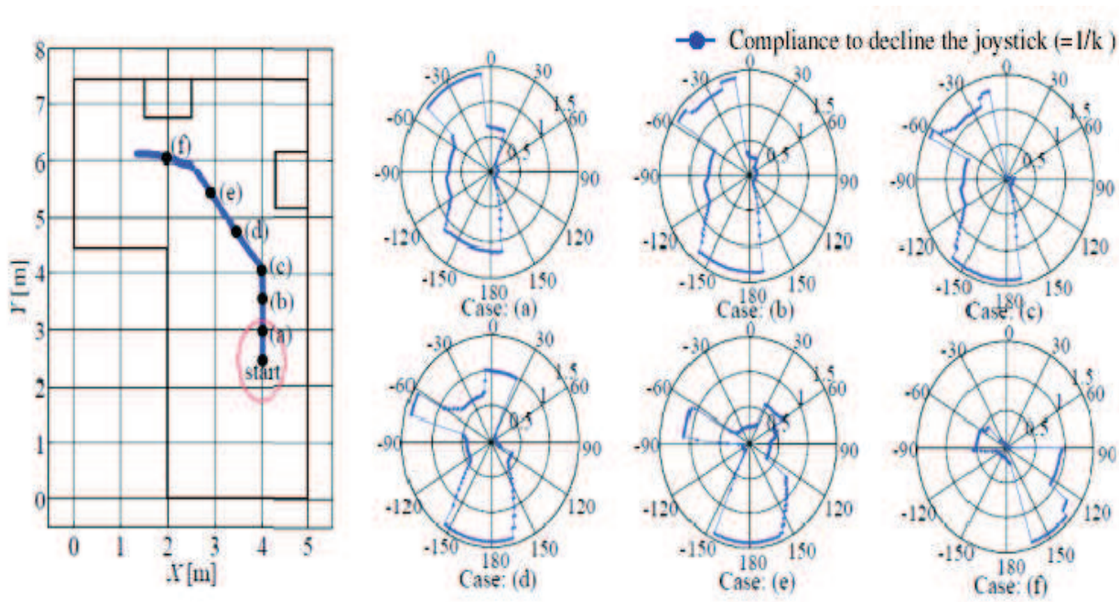

Fig. 19. Experimental result with the change of joystick's compliance during running of OMW.

Figure 19 shows the facilitation (= 1/*k*) to operate joystick for the corresponding orientation of the joystick. Then, OMW runs the speed of 0.4 [m/s]. In the sense of global coordinate as shown in the right side of Fig. 19 (case(a)-(f)), forward direction is 0 [deg], backward direction is 180 [deg], right direction is 90 [deg], and left direction is -90 [deg]. Note that, in the case that the OMW is moving in the direction nearing the obstacle, it is difficult to decline the joystick, because the motor torque grows. In other cases, it is easy to decline the joystick. Therefore the operator can naturally find out about existing obstacle and danger of collision by the present haptic device.

In the previous paragraphs, the haptic feedback joystick informs the danger level of collision to the operator. Additionally, in this section, the navigation guidance system that enable the operator to navigate the moving of OMW in the direction without crashing into obstacle, is built. This system is called the navigation guidance haptic feedback system. To begin with, take a look at the closest layer existing the recognition point.

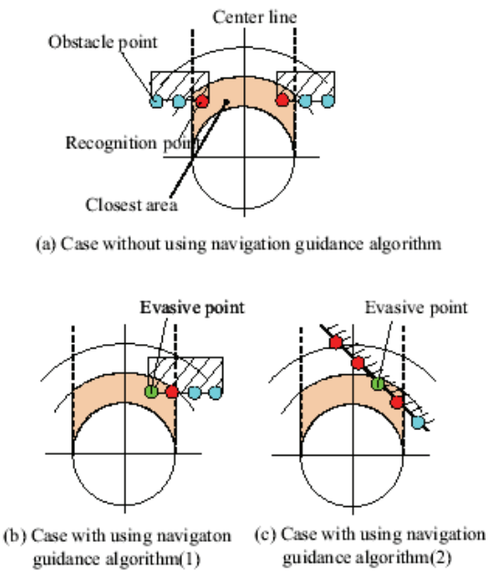

Fig. 20. Classification of cases with and without using navigation assistance algorithm

The recognition area in this closest layer is defined as the closest area, as shown in Fig. 20. Then, if the recognition points exist across the center line in the closest area, as shown in Figure 20 (a), the navigation guidance haptic feedback system is not conducted. On the other hand, if the recognition points exist on one side, as shown in Figure 20 (b) and (c), the navigation guidance haptic feedback system is worked. Moreover, in these cases (for example Figure 20 (b),(c)), the recognition points are described by polar coordinate system, and the recognition point possessing the minimum polar angle is defined as the evasive point.The OMW is controlled to move in the direction Φ by the operator's input force with the joystick, as shown in Fig. 21 (a). Using the recognition area defined previously, the inductive angle Ω_d with joystick is required, as shown in Fig. 21. Then the scale of Y-axis is altered, therefore, dash attached with variable indicates the changing of X-Y axis scale. For example, the evasive point is acquired in the Nth layer L_N (layer number is $n = N$), as shown in Figure 21 (b). In this case, the evasive point E' exists in the right side of the recognition

area divided by the center line. The evasive point $E'(d_e'; q_e')$ is described by polar coordinate system which has the origin of coordinate is the center of the vehicle area. This system automatically gives a force to decline joystick in the direction without existing obstacle, regardless of operator's intention. The vector of the automatically given force is defined as the inductive force F_d, and the sum of vector of the inductive force F_d and operator's current input force F_i is defined as the evasive force F_e, as shown in Fig. 21 (a).

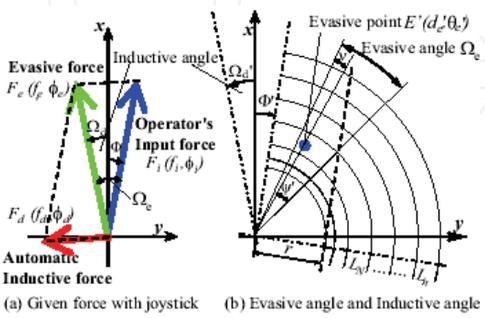

Fig. 21. Proposed method of the automatic inductive force for navigation-assistance.

These vectors are also described by polar coordinate system. The magnitude of vector of operator's current input force f_i is equal to τ witch is derived by the Eq. (16) and (17), therefore, the polar coordinate f_i and q_i are described as

$$f_i = \tau, \qquad \varphi_i = \Phi \tag{18}$$

The difference between the maximum angle range of the closest area defined by the Eq. (15) and the angle of the evasive point is described as

$$\Psi' = \sin^{-1}\left(\frac{r + Nl}{r}\right) - \theta_e' \tag{19}$$

In the case that the evasive point exists in the left side of the recognition area divided by the center line, Ψ′ is

$$\Psi' = -\sin^{-1}\left(\frac{r + Nl}{r}\right) + \theta_e' \tag{20}$$

The evasive angle Ω_e' is described as

$$\Omega_e' = \Psi' + v, \tag{21}$$

where ν is constant number for safe evasive movement and ν = 0.0872. The inductive angle

Ω_d' is described as

$$\Omega_d' = \Phi' + \Omega_e', \tag{22}$$

The inductive angle Ω_d is reconverted in to the transformed scale of X-Y axis of Ω_d' as following equation.

$$\Omega_d = \tan^{-1}\left(\frac{\sin\Omega_d'}{d_b / d_a \cdot \cos\Omega_d'} \right) \tag{23}$$

Therefore, the evasive force $F_e(f_e, \phi_e)$ is described as

$$f_e = f_i, \quad \phi_e = \Omega_d \tag{24}$$

where the magnitude of the evasive force f_e is as the same as the magnitude of the operator's current input force f_i in order to uphold OMW's velocity of pre-inducting and past-inducting. And the angle of the evasive force ϕ_e is determined in order to get out the evasive point from recognition area. Next, the polar coordinate f_e and ϕ_e are converted into the Cartesian coordinates f_{ex} and f_{ey}, as follows.

$$f_{ex} = f_e \cos\phi_e, \quad f_{ey} = f_e \sin\phi_e \tag{25}$$

Also f_i and ϕ_i are converted to the Cartesian coordinates f_{ix} and f_{iy},as follows.

$$f_{ix} = f_i \cos\phi_i, \quad f_{iy} = f_i \sin\phi_i \tag{26}$$

Therefore the inductive force $F_{d(}\, f_{dx}; f_{dy)}$ is obtained by the following equations, because the evasive force F_e is the sum of vector of the inductive force F_d and operator's current input force F_i.

$$f_{dx} = f_{ex} - f_{ix}, \quad f_{dy} = f_{ey} - f_{iy} \tag{27}$$

The inductive force F_d is given to the motors attached on the joystick, in addition to given the force τ described by Eq. (16).

The OMW is set at the position of 2 [m] away from the obstacle, and the obstacle is closed to the OMW, as shown in Fig. 22. The OMW's wheels are run idle, the joystick is declined toward forward, and OMW's input velocity is 0.4 [m/s]. The inductive force given to the joystick is automatically provided. Figure 19 shows the experimental result of inductive

navigation guidance system, blue point describes the evasive point and green line describes the evasive force.

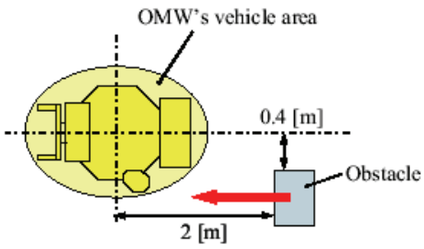

Fig. 22. Experimental condition of the proposed inductive navigation assistance system

As obstacle is approached OMW, the evasive angle is larger, and the force τ given to resist declination of the joystick by Eq. (16) is larger, so the operator's input force also is larger. Therefore, as seen from this figure, the evasive force with is the sum of vector of the inductive force F_d and operator's current input force F_i is appropriately given to the navigator. Then, following the inductive force which given to provide the joystick with the evasive force, the navigator can evade the obstacle. So good navigation-assistance could by achieved. The effectiveness of the proposed assistance system was demonstrated through a lot of experiments.

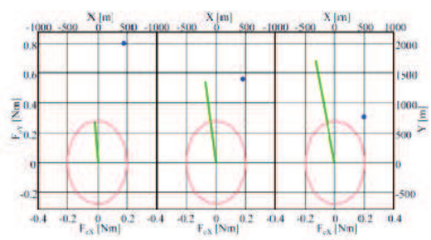

Fig. 23. Experimental results of the proposes inductive navigation assistance system.

4. Power Assist Control of OMW for Helper

The force of the attendant is applied to the handles of the OMW shown in Fig. 24 (a). This force is then measured by the 6-axis force sensor shown in Fig. 24 (b).

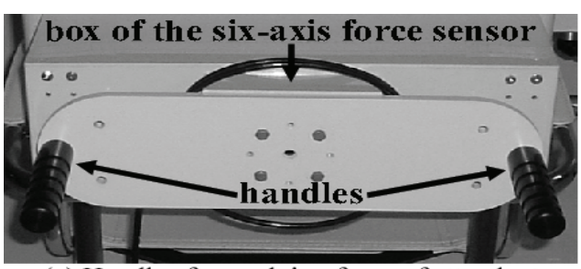

(a) Handles for applying force of attendant

(b) 6-axis force sensor

Fig. 24. Position of the handles of the OMW and 6-axis force sensor

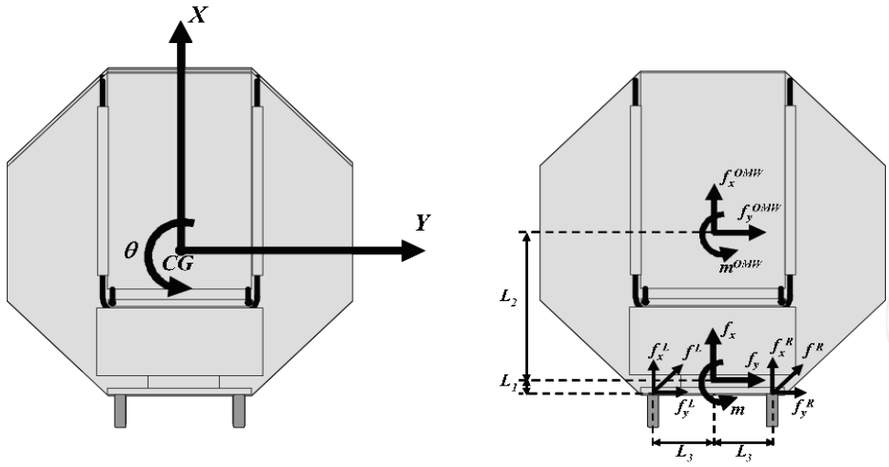

(a) Coordinate system of the OMW. (b) Decomposition of the forces applied to the handles of the OMW.

Fig. 25. Decomposition of the force applied to the handles of the OMW

The force applied to the handles of the OMW must be decomposed according to the directions shown in Fig. 7 (a). In Fig. 10 (a), θ represents an axis perpendicular to the plane determined by X and Y. The OMW rotates around this axis in a CW or a CCW direction. The force applied to the handles in the direction X, f_x, and the force applied to the handles in the direction Y, f_y, shown in Fig. 10 (b), are decomposed according to the following equations:

$$f_x = f_x^L + f_x^R \tag{28}$$

$$f_y = f_y^L + f_y^R \tag{29}$$

As there is a perpendicular distance L_3 between the center of the force sensor and the forces and $\mathbf{f}_x^L$, and $\mathbf{f}_y^L$ a perpendicular distance L_1 between the center of the force sensor and the forces $\mathbf{f}_y^L$ and $\mathbf{f}_y^R$, these forces produce a momentum with respect to the center of the force sensor. This momentum is given as:

$$m = \left(f_x^R - f_x^L\right)L_3 + \left(f_y^L + f_y^R\right)L_1 \tag{30}$$

In order to represent the movement of the OMW, the forces and the momentum shown in Eq. (28), Eq. (29) and Eq. (30), must be translated to the center of the OMW, as shown in Fig. 25 (b). This is accomplished by the following equations:

$$f_x^{OMW} = f_x \tag{31}$$

$$f_y^{OMW} = f_y \tag{32}$$

$$m^{OMW} = m + f_y L_2 \tag{33}$$

As shown in Eq. (33), the rotation of the OMW is influenced by the force in the lateral direction Y. This observation will be used later when explaining the navigation direction estimator for force input.
The force input by the attendant is then converted to a reference velocity for the OMW by using a first-order lag controller. The reference velocity is proportional to the input force. This means that the attendant can move the OMW by the same force even when the weight of the occupant or the inclination of the travel surface changes. Moreover, the OMW can stop when the attendant stops pushing. The output signal of the force sensor, considered $F = [f_x, f_y, m_\theta]^T$, is converted to the reference velocity V_{OMW} of the OMW by a first-order lag controller.

Fig. 26. Touch panel of OMW.

A touch panel is a display device that accepts user input by means of a touch sensitive screen. Because of their compact nature and ease-of-use, touch panels are typically deployed for user interfaces in automation systems, such as high-end residential and industrial control. Touch panels are also becoming common on portable computers such as Tablet PCs, Ultra-Mobile PCs and consumer devices such as VOIP phones. In the OMW, a touch panel as shown in Fig. 26 is used as an input device in which the attendant of the OMW draws the desired direction of motion. As shown in Fig. 11, the touch panel is mounted in the rear part of the OMW such as the attendant can reach to it easily. The touch panel used in the OMW is a TFT Touch Monitor HV-141T produced by ULTEC Corporation, Japan.

The first-order lag controller converts the output signal of the force sensor $F = [f_x, f_y, m_\theta]^T$ to the reference velocity $V_{OMW} = [V_x, V_y, \omega]^T$ of the OMW. The input force can be converted to the reference velocity by using a first-order lag controller that contains an integral element.

$$G_i(s) = \frac{V_i(s)}{F_i(s)} = \frac{K_i}{T_i s + 1} \quad (i = x, y, m) \tag{34}$$

The reference velocity V_{OMW} exponentially converges to zero by using this controller when the attendant stop pushing the handle. If the time constant T_i is too small, the effect of vibration of input force or noise becomes large. If the time constant T_i is too large, the manipulability of the OMW degrades because of its slow response. The parameters of the first-order lag controller were determined by trial and error as $K_x = 0.0003$, $K_y = 0.0002$, $K_m = 0.0007$, $T_x = 0.6$, $T_y = 0.75$ and $T_m = 0.75$. A block diagram of the system is shown in Fig. 27.

When a first-order lag controller is used for the transformation from force to velocity (Kitagawa et al., 2004), a large jerk (derivative of acceleration) occurs if the input force changes suddenly. This jerk is considered a factor very significant to riding comfort. For the improvement of riding comfort this jerk must be diminished. A method for diminishing the magnitude of this jerk is proposed as follows:

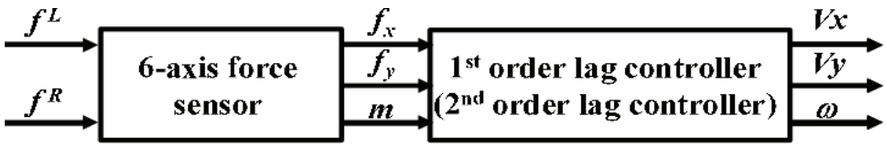

Fig. 27. Block diagram of the power-assist system

1. The gain K_i (i = x, y, ω) is decreased.
2. The value of the time constant T_i (i = x, y, ω) is increased.
3. The largest restriction of the jerk is established.
4. The controller is modified.

In item 1, as the output velocity related to the help force decreases, the jerk becomes small too. However, a large force is necessary for achieving the desired velocity. The effect of power-assist then fades and the OMW becomes, once again, very heavy for the attendant.
In items 2 and 3, the jerk can be made smaller too, but in this case, after the change, the time necessary for reaching the desired velocity increases. This generates a problem of deterioration of operability. In other words, the proposed method provides improvement in riding comfort, but the OMW's operability decays. Thus, a second-order lag controller

$$G_i(s) = \frac{V_i(s)}{F_i(s)} = \frac{K(\omega_n)_i^2}{s^2 + 2\zeta_i(\omega_n)_i s + (\omega_n)_i^2} \quad (i = x, y, m) \tag{35}$$

is chosen as a power-assist controller which can provide compatibility between both operability and riding comfort. Here, ζ is the attenuation factor. Even when the force added by attendant is fixed, if overshoot O_s occurs, a certain amount of time is required for the velocity to achieve convergence and therefore operability declines during this period. Thus, in order to avoid overshoot, ζ(i = x, y, m) is chosen as $\zeta_x = 1$, $\zeta_y = 1$, $\zeta_m = 1$. In addition, $T_x = 0.4$, $T_y = 0.4$, and $T_m = 0.4$, is used.
On the other hand, in the case of the second-order lag controller, ω_n is determined such that the system is not influenced by the noise included in the input and good operability of

OMW is also obtained. Thus, in this case, ω_n is chosen by trial and error as $(\omega_n)_x = 4$, $(\omega_n)_y = 4$, and $(\omega_n)_m = 4$.

An experimental comparison of the jerk produced in the X direction by a first-order lag controller and a second-order lag controller, each at the same reference velocity, was conducted. The experimental parameters were $K_x = 0.02$, $T_x = 0.4$, $\zeta_x = 1.0$, $(\omega_n)_x = 4.0$, and sampling time $t_s = 0.03$ [s]. OMW was moved in automatic mode. Jerk was evaluated by differentiating the output of the encoders of the OMW's motors. Experimental results are shown in Fig. 28. V_x is the reference velocity, and j_x^{OMW} shows the actual jerk that was calculated by using the encoders' output.

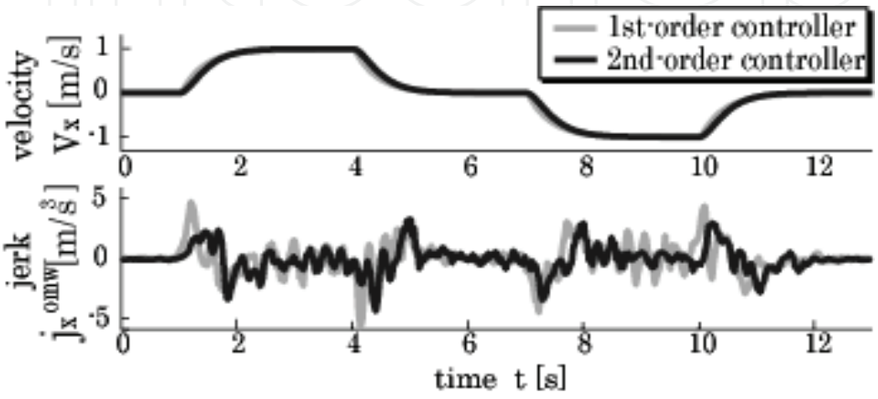

Fig. 28. Experimental results of experiments for measuring the jerk

Since in order to calculate the jerk using the encoders' output this output must be differentiated, the problem occurs that even a small amount of noise present in the encoders' output will case big changes in the jerk's value due to differentiations. Here, instead of concentrating on very precise values of the jerk, attention is given to the big variations in the jerk, so using the jerk's values for (t-1) and (t+1), where "t" is the actual time, the jerk's moving average is calculated. As the velocity is constant between t = 3~4 [s], the jerk observed in this time interval of is due to the erratic reading of encoders and is therefore ignored. Attention will be focused on the interval of time between t = 1~2 [s], in which there occurs acceleration and deceleration. It has been verified that a second-order lag controller can achieve a maximum reduction of 20% of the jerk's value produced during this period. Improvement of riding comfort is then assured by using a second-order lag controller. Moreover, comparing this result with the case in which the reference velocity is input to a first-order lag controller, there is almost no delay of time response and thus operability is not degraded. For these reasons, it is possible to conclude that in this case the second-order lag controller obtains greater performance than does the first-order lag controller. In addition, as riding comfort depends on the subjective judgment of the OMW's occupant, riding comfort was evaluated by using the Semantic Differential (SD) method. The OMW was made to move in automatic mode in X and Y directions, and a questionnaire consisting of 7 items related to driving comfort was presented to 10 different chair users. The mean value of the results obtained in each item are shown in Fig. 29 (a) for the X direction and Fig. 29 (b) for the Y direction. Even when the difference in the results in the X direction and the Y direction is not so significantly large, it is possible to see that the values obtained by the

second-order lag controller are much better than those obtained by the first-order lag controller. Thus, a second-order lag controller will be used as the power-assist controller due to its improvement in riding comfort. Then, in the block diagram of Fig. 26, a second order lag controller is used instead of the first order lag controller.

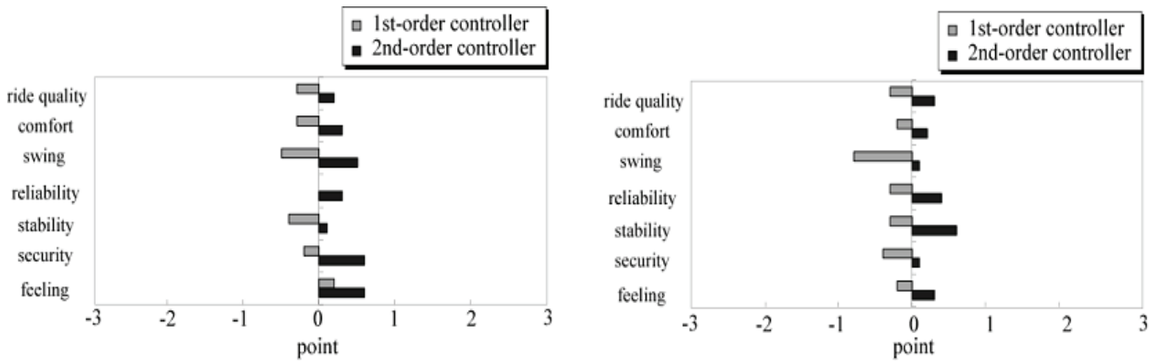

(a) X direction (b) Y direction

Fig. 29. Results of questionnaire when the OMW moves in the X direction and Y direction

5. Adaptive control by Neuro-Fuzzy System of OMW Using a Touch Panel as Human Interface for Realizing Tailor-made vehicle

When the attendant tries to rotate the OMW around its gravity center, CG, the OMW begins to slide and the radius of rotation becomes very large, as shown in Fig. 30. In this figure, the octagon represents the OMW, and the circle inside the octagon is the trajectory that point "A" in the periphery of the OMW, would describe if the OMW rotates perfectly over the CG. The thick dark line represents the trajectory of the CG, while the thin gray line represents the trajectory of "A". The numbers in arithmetic progression show how the OMW changes its position. All the symbols, lines and colors used in Fig. 30 regarding simulations and experimental results will indicate the same meanings in all the figures that follow throughout the remainder of the text.

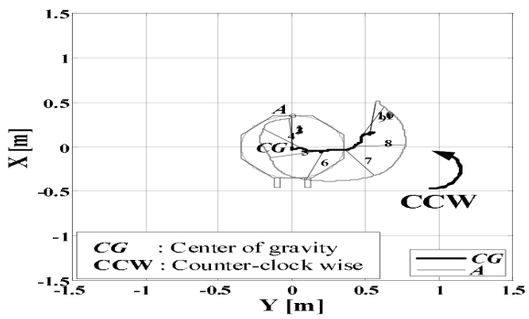

Fig. 30. A case of rotational movement of OMW in counter-clockwise (CCW) direction, when just power-assist is used

Rotation around the CG is very difficult because the OMW's rotation is not pure rotation, but is also influenced by any force that acts in the lateral direction, as shown. A survey was conducted among various attendants trying to discover some relationships in the way they realized forwards-backwards, lateral, and rotational movements. The goal of the survey was to find general rules that drew a relationship between the three described motions. Though it was impossible to find general rules that explained all cases, a relationship was found between lateral and rotational movements. It was found that if the movement in the forward or backward direction is not considered, when most of the attendants want to:

a) rotate in a clockwise (CW) direction, in addition to the rotational momentum they use some force in the lateral left direction.
b) rotate in a counter-clockwise (CCW) direction, in addition to the rotational momentum they use some force in the lateral right direction.
c) move in a lateral right direction, in addition to the lateral force they use some momentum in the CW direction
d) move in a lateral left direction, in addition to the lateral force they use some momentum in the CCW direction

1	If	$\omega < 0$ and $Vy < 0$,	then	$\omega < 0$
2	If	$\omega > 0$ and $Vy > 0$,	then	$\omega > 0$
3	If	$Vy > 0$ and $\omega < 0$,	then	$Vy > 0$
4	If	$Vy < 0$ and $\omega > 0$,	then	$Vy < 0$
5	If	$\omega < 0$ and $Vy \approx 0$,	then	$\omega < 0$
6	If	$\omega > 0$ and $Vy \approx 0$,	then	$\omega > 0$
7	If	$Vy > 0$ and $\omega \approx 0$,	then	$Vy > 0$
8	If	$Vy < 0$ and $\omega \approx 0$,	then	$Vy < 0$
9	If	$Vy \approx 0$ and $\omega \approx 0$,	then	0

Table 2. Fuzzy inference system

According to the traditional convention, CCW rotation is considered to be produced by a positive angular velocity $\omega > 0$, rotation in CW direction is considered to be produced by a negative angular velocity $\omega < 0$, lateral movement to the right is considered to be produced by a positive lateral velocity $V_y > 0$ and lateral movement to the left is considered to be produced by a negative lateral velocity $V_y < 0$. Following what has been established in the previous paragraphs, it is possible to construct Table 2. The system shown in Table 2 can be appropriately represented by a Takagi-Sugeno-Kang fuzzy model (Sugeno & Kang, 1998), (Takagi & Sugeno, 1985), with appropriate membership functions for the input, and the output being a function of the inputs, such as:

$$y_i = A_i \times V_{yj} + B_i \times \omega_j + C_i \quad (36)$$

where y_i represents the output function, "i" is a sub-index that indicates the rule to which the coefficients correspond, and the sub-index "j" can take any value in the set {Negative, Zero, Positive}.Then, by rearranging the rules of Table 2, and using the output function y_i, the system described in Table 2 becomes as shown in Table 3.

R	Antecedent		Consequent
1	If $Vy < 0$ and $\omega < 0$,	then	$y_1 = A_1 \times Vy_N + B_1 \times \omega_N + C_1$
2	If $Vy \approx 0$ and $\omega < 0$,	then	$y_2 = A_2 \times Vy_Z + B_2 \times \omega_N + C_2$
3	If $Vy > 0$ and $\omega < 0$,	then	$y_3 = A_3 \times Vy_P + B_3 \times \omega_N + C_3$
4	If $Vy < 0$ and $\omega \approx 0$,	then	$y_4 = A_4 \times Vy_N + B_4 \times \omega_Z + C_4$
5	If $Vy \approx 0$ and $\omega \approx 0$,	then	$y_5 = A_5 \times Vy_Z + B_5 \times \omega_Z + C_5$
6	If $Vy > 0$ and $\omega \approx 0$,	then	$y_6 = A_6 \times Vy_P + B_6 \times \omega_Z + C_6$
7	If $Vy < 0$ and $\omega > 0$,	then	$y_7 = A_7 \times Vy_N + B_7 \times \omega_P + C_7$
8	If $Vy \approx 0$ and $\omega > 0$,	then	$y_8 = A_8 \times Vy_Z + B_8 \times \omega_P + C_8$
9	If $Vy > 0$ and $\omega > 0$,	then	$y_9 = A_9 \times Vy_P + B_9 \times \omega_P + C_9$

Table 3. Takagi-Sugeno-Kang fuzzy model

Vy	Range	ω	Range
$Vy < 0$	[-1.0 ~ -0.1)	$\omega < 0$	[-3.30 ~ -0.20)
$Vy \approx 0$	[-0.1 ~ 0.1]	$\omega \approx 0$	[-0.20 ~ 0.20]
$Vy > 0$	(0.1 ~ 1.0]	$\omega > 0$	(0.20 ~ 3.30]

Table 4. Range of velocities

The Lateral velocity V_y is in the range [-1 ~ 1], and the angular velocity ω is in the range [-3.3 ~ 3.3]. The units of V_y and ω are [m/s] and [rad/s], respectively. After much trial and error, it was found that the more appropriate values for (V_y < 0), (V_y ~ 0), (V_y > 0), (ω < 0), (ω ~ 0), and(ω > 0), correspond to the ranges shown in Table 4.

The functions used for the partitions of the total range of V_y and ω are called dsigmoidal functions (Mathworks, 2002), and are defined as the difference of two sigmoidal functions. That is, if Eq. 26 is a sigmoidal function, with input data "x", and parameters "a" and "c", where "a" defines the inclination of the curve in the crossover point "c". Crossover points are defined (Jang et al., 1997), as the points in which "μ" = 0.5. Depending on the sign of the parameter "a", the sigmoidal membership function is inherently opened to the right or to the left (if "a" is positive, the sigmoidal function is opened to the right, and if "a" is negative the sigmoidal function is opened to the left).

$$f(x, a, c) = \frac{1}{1 + e^{-a(x-c)}} \tag{37}$$

A dsigmoidal function can be defined as

$$f(x, a_1, c_1) - f(x, a_2, c_2) = f(x, [a_1, c_1, a_2, c_2]) \quad (38)$$

The partitions of the ranges of V_y and ω by using dsigmoidal functions are shown in Fig. 31.

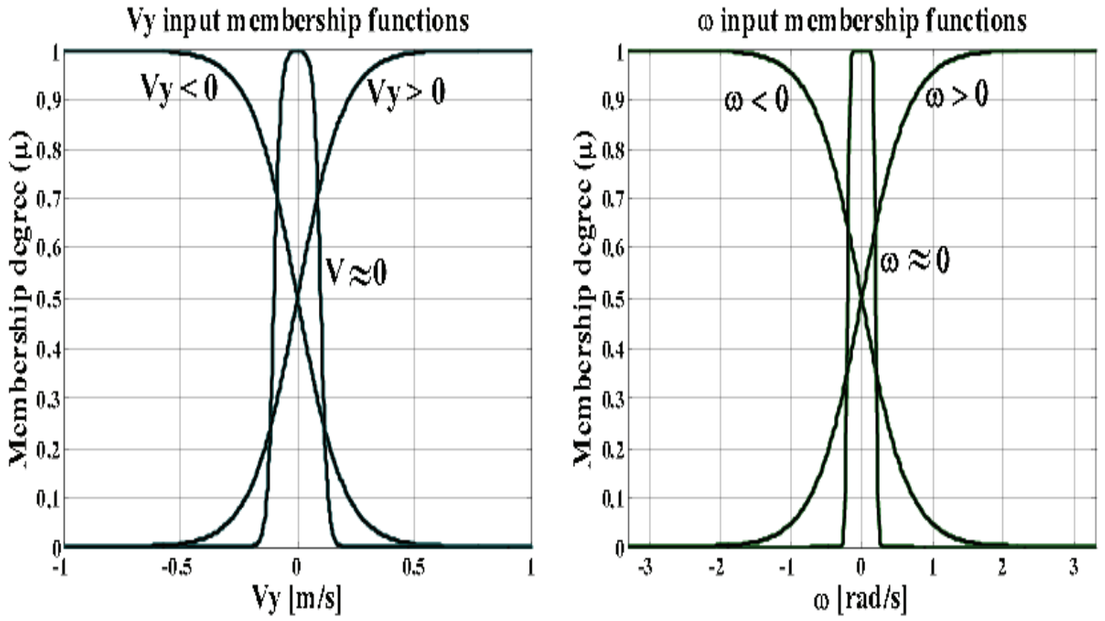

Fig. 31. Partitions of the ranges of V_y and ω by using dsigmoidal functions

R	A	B	C
1	0.05	1	0
2	0	1	0
3	1	0.05	0
4	1	0	0
5	0	0	0
6	1	0	0
7	1	0.05	0
8	0	1	0
9	0.05	1	0

Table 5. Values of the coefficients A, B and C

The coefficients "A" and "B" are decided considering the values shown in Table 2. C is always 0. The values of "A_i", "B_i" and "C_i" are shown in Table 5. The value "0.05" was hosen by trial and error. The reason for choosing "0.05" instead of "0", as could be inferred rom Table 2, is in order not to cancel completely the movement in the undesired direction. igger values, such as "0.1", "0.2", ... , have been tested as well, but it has been found that if alues greater than "0.05" are used, the deviation in direction Y is not reduced as much as desired. In fact, for obtaining the value of the desired lateral velocity V_y and the desired ngular velocity ω, two fuzzy reasoning systems are needed. The inputs are the same, but the outputs are decided as shown in Table 6. These two fuzzy systems will be used in the block labeled "directional reasoning" in the block diagram of the OMW system shown in Fig. 32. The contents of the block "directional reasoning" are shown in Fig. 33.

Rule	Antecedents	Consequents					
		$\hat{V}y$			$\hat{\omega}$		
		A^{Vy}	B^{Vy}	C^{Vy}	A^{ω}	B^{ω}	C^{ω}
1	If $Vy < 0$ and $\omega < 0$, then	0 (Vy)	0 (ω)	0	0.05 (Vy)	1 (ω)	0
2	If $Vy \approx 0$ and $\omega < 0$, then	0 (Vy)	0 (ω)	0	0 (Vy)	1 (ω)	0
3	If $Vy > 0$ and $\omega < 0$, then	1 (Vy)	0.05 (ω)	0	0 (Vy)	0 (ω)	0
4	If $Vy < 0$ and $\omega \approx 0$, then	1 (Vy)	0 (ω)	0	0 (Vy)	0 (ω)	0
5	If $Vy \approx 0$ and $\omega \approx 0$, then	0 (Vy)	0 (ω)	0	0 (Vy)	0 (ω)	0
6	If $Vy > 0$ and $\omega \approx 0$, then	1 (Vy)	0 (ω)	0	0 (Vy)	0 (ω)	0
7	If $Vy < 0$ and $\omega > 0$, then	1 (Vy)	0.05 (ω)	0	0 (Vy)	0 (ω)	0
8	If $Vy \approx 0$ and $\omega > 0$, then	0 (Vy)	0 (ω)	0	0 (Vy)	1 (ω)	0
9	If $Vy > 0$ and $\omega > 0$, then	0 (Vy)	0 (ω)	0	0.05 (Vy)	1 (ω)	0

Table 6. Partitions of the systems shown in Table 3 in two sub-systems

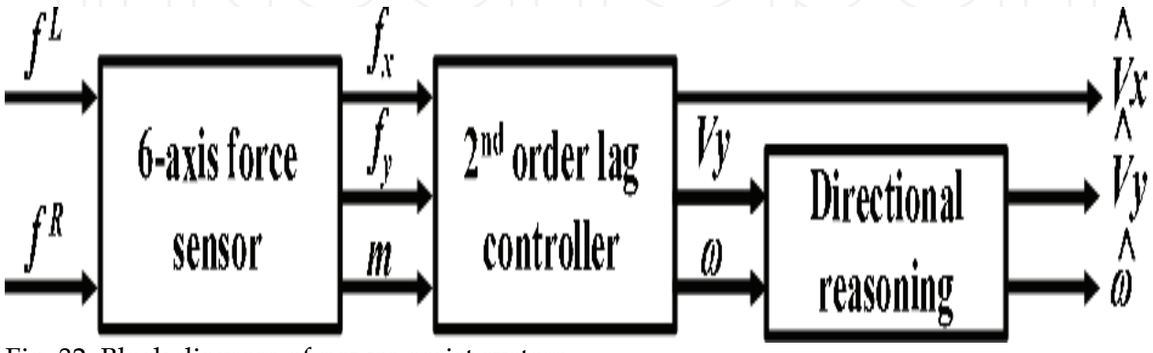

Fig. 32. Block diagram of power-assist system

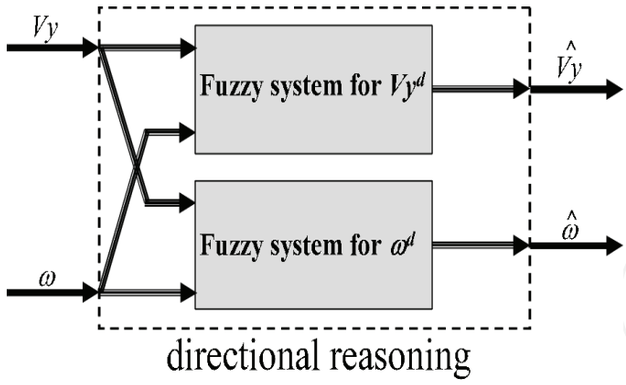

Fig. 33. Contents of the block "directional reasoning" in Fig. 32.

The effectiveness of the fuzzy system described above was tested experimentally. After much trial and error, the values of $K(\omega_n)_i$ in Eq. (35), were determined to be: $K(\omega_n)_x = 0.19$, $K(\omega_n)_y = 0.22$, and $K(\omega_n)_\omega = 1.1$, with $\zeta_i = 1$ and $(\omega_n)_i = 4$. Experiments were conducted for four different attendants by using a fuzzy reasoning system tuned to respond to the characteristics of one of them. The attendants were asked to move the OMW laterally, backwards, and forwards, in CCW rotation, and in the diagonal direction. The results obtained for the 4 attendants in the case of CCW rotation are shown in Fig. 34. As shown in Fig. 20, even when the Fuzzy Reasoning (FR) System helps to improve the OMW's operability, the result is different for each attendant because of the particular characteristics of each of them. According to the results shown in Fig. 34, it is clear that the fuzzy reasoning system was tuned to respond to the characteristics of "Attendant 3" and for that reason the lateral deviation is almost nonexistent in his case. As "Attendant 3" does not use so much force in the not adjusted X direction, then he can rotate almost perfectly over the CG of the OMW. For the other three cases, the not precise tuning for rotation and lateral movement, combined with the effect of the force in direction X, causes that the movement is not as good as expected. As a consequence of the analysis of these results, the idea of tuning the fuzzy system according to the characteristics of each attendant came into view. The tuning by trial and error is time consuming and requires many attempts by the attendants who may grow tired or bored. Therefore, another method of tuning the FR system must be found. Using the input data of the attendants is the most natural alternative. In this case, the FR systems will tune automatically by learning the tendency of the different attendants. As the FR systems do not have an ability to learn, the addition of a complementary system that allows learning is necessary. Learning capability can be obtained by adding a Neural Network (NN) to the FR system. A hybrid system called a neuro-fuzzy system is then obtained. Much research exists regarding this topic (Jang, 1993), (Jang et al., 1997), (Juang & Lin, 1998), (Lian et al., 1999), (Lin & Lee, 1991), (Nguyen et al., 2003). Jang (Jang, 1993), (Jang et al., 1997), developed the ANFIS (Adaptive-Network-based Fuzzy Inference System), a neuro-fuzzy system in which the fuzzy inference system is tuned by using the system's input data. The tuning is performed by minimizing the output error of the NN used in combination with the fuzzy inference system. For achieving this goal, the NN is trained by using a hybrid method that combines least squares and the Backpropagation algorithm (BP law). This method is thus thought to be effective as a parameter tuning method for the OMW's fuzzy inference system.

The ANFIS was proposed as a system that can tune a FR system through the use of input data. First, the FR system is changed to the form of a NN network that can be trained by using the system's input data. Fig. 35 shows the ANFIS system used for obtaining the value of the desired angular velocity and the desired lateral velocity. This system is based on the Takagi-Sugeno-Kang fuzzy models shown in Table 6. The ANFIS system shown in Fig. 36 has 5 layers. The nodes of the layers are represented by circles or squares. Square nodes contain values which can be tuned. Circular nodes contain fixed values or mathematical operators. A brief explanation of how the different layers shown in Fig. 36 are achieved follows. For a more detailed explanation in this topic, and in the training of the ANFIS, refer to references (Jang, 1993), (Jang et al., 1997).

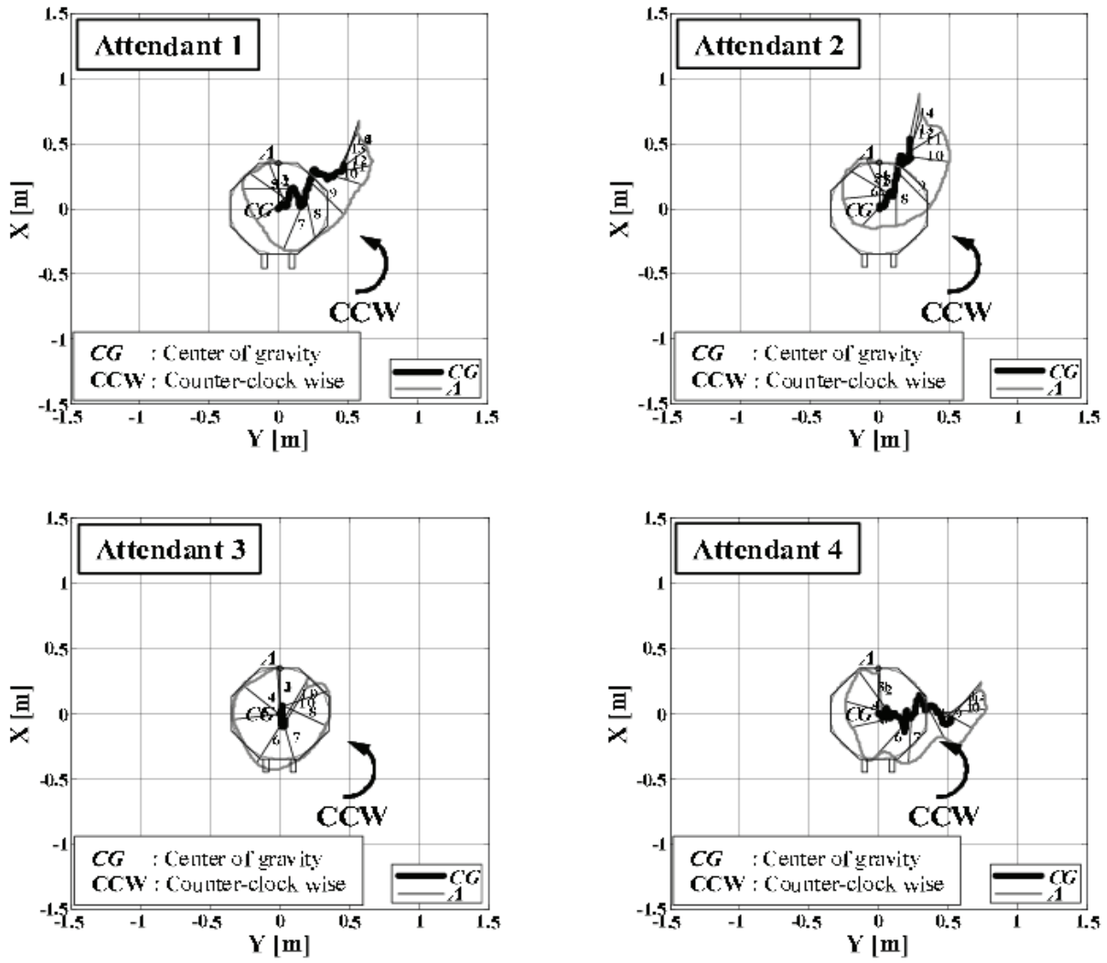

Fig. 34. Experimental results of four attendants when the Fuzzy Reasoning system is used

- 1st Layer: Here the inputs V_y and ω are subjected to the action of the membership functions of Fig. 31, which are represented by its parameters (a_1 … a_{12}) and (c_1 … c_{12}).
- 2nd Layer: In the 2nd Layer the fuzzy rules shown in Table 6 are constructed. As the

antecedents are jointed by a logic "AND", this relationship is mathematically obtained by the product (Π) of the two antecedents. The output of each node represents the firing strength of a rule, which is represented by α_i (i = 1, ... , 9).

- 3rd Layer: This is a normalization layer, where the ratio of the ith rules' firing strength to the sum of all rules firing strength is calculated.
- 4th Layer: Here the normalized firing strength that comes from the 3rd Layer is multiplied by the output functions of the fuzzy reasoning system.
- 5th Layer: The overall output of the system is computed as the sum of all the incoming signals.

In previous research (Terashima et al., 2004), the desired direction of motion of the attendant was input by using the keyboard of the computer of the OMW. However, the attendant could not get a clear idea of the direction in which he wanted to move, neither verify if the real motion of the OMW really corresponded to his desire. In order to provide the attendant with an easy way for inputing the desired direction of motion and for verifying the direction of motion, a human interface consisting of touch panel, as shown in Fig. 26 is used. A GUI (Graphical User Interface) was developed for making easy the interaction with the attendant, as show in Fig. 36. In this GUI the attendant can draw any kind of motion, be it an slanting motion, or a rotational movement. Moreover, the GUI allows the attendant to follow the motion of the OMW and realize the difference between the desired and the real motion of the OMW.

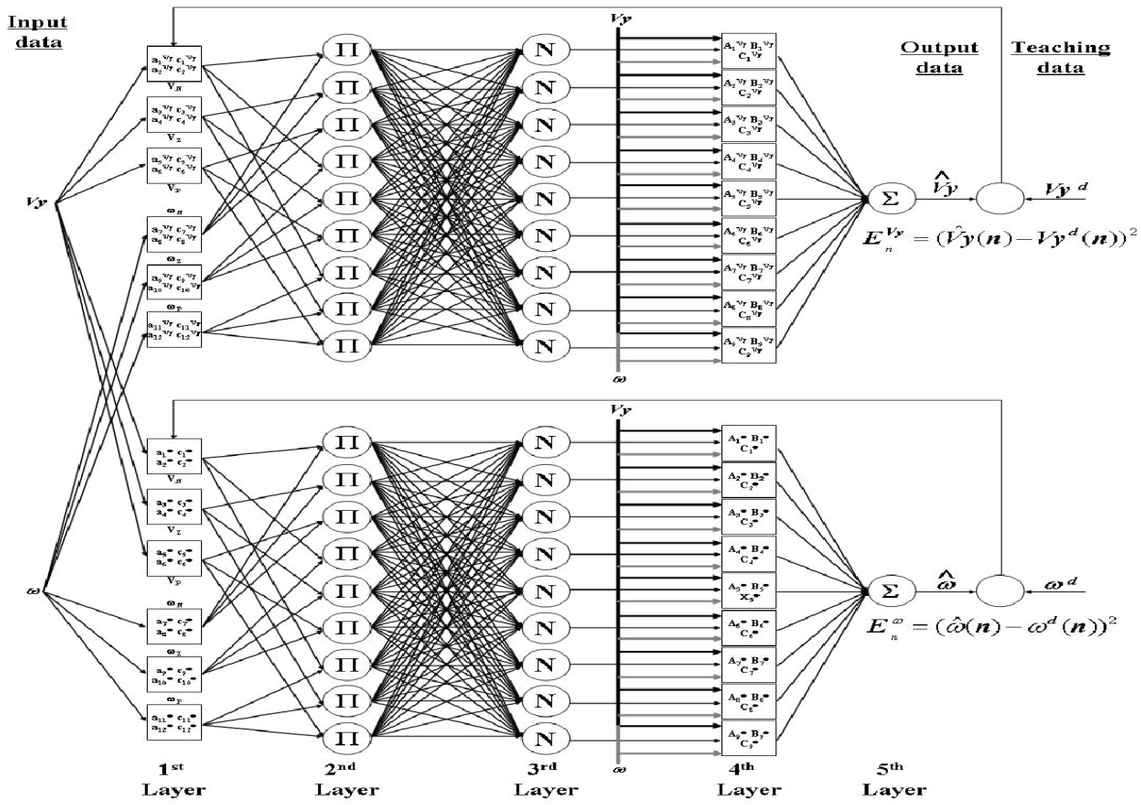

Fig. 35. The ANFIS system

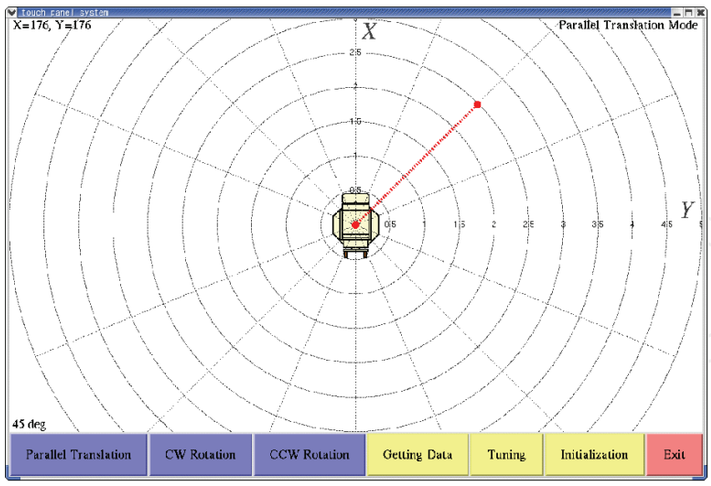

Fig. 36. GUI developed for the touch panel

The procedure for applying the touch panel is as follows:

a) First, the attendant draws in the touch panel the kind of movement that he desires to accomplish.
b) Then, the attendant moves the OMW trying to accomplish the desired motion.
c) However, in the general case, there as a difference between the desired motion and the real motion. This difference is used for the training of the ANFIS system of the OMW, as explained in (Terashima et al., 2004).

A Reduction Multiplicative Factor (RMF) which decreases the value of V_x in the case of rotational motion, and keeps it unchanged in the case of forwards-backwards movement was the solution provided by authors (Urbano et al., 2006a) for improving the forwards-backwards motion, lateral motion and rotational motion over the gravity center of the OMW.
However, as V_y was subjected to fuzzy reasoning and V_x was not, it was not possible to achieve good operability for slanting motions, like diagonal motion. In the case of diagonal motion, for example, the attendant tries to move the OMW in such a way that the inputs of V_x and V_y are almost the same in the beginning. Nevertheless, as V_y is subjected to directional reasoning, its value changes. V_x is not subjected to directional reasoning, then its value remains always the same. As a consequence, it is not possible to achieve good operability in diagonal motion.
For solving this problem, V_x was subjected to directional reasoning too using the fuzzy rules shown in Table 7 These rules make it possible to include V_x in the fuzzy reasoning system without disturbing the values of V_y or ω. The block diagram of the system that considers power assist and fuzzy reasoning is shown in Fig. 37, and the contents of the block labeled as "directional reasoning" are shown in Fig. 38. By including V_x in the ANFIS system it was possible to accomplish a general omni-directional motion. Then, the complete ANFIS of the OMW becomes as shown in Fig. 39, and the complete system, when the touch panel is included, is shown in Fig. 40.

R	Antecedent	Consequent
1	If $Vx < 0$ and $Vy < 0$,	then $Vx < 0$
2	If $Vx \approx 0$ and $Vy < 0$,	then $Vx \approx 0$
3	If $Vx > 0$ and $Vy < 0$,	then $Vx > 0$
4	If $Vx < 0$ and $Vy \approx 0$,	then $Vx < 0$
5	If $Vx \approx 0$ and $Vy \approx 0$,	then 0
6	If $Vx > 0$ and $Vy \approx 0$,	then $Vx > 0$
7	If $Vx < 0$ and $Vy > 0$,	then $Vx < 0$
8	If $Vx \approx 0$ and $Vy > 0$,	then $Vx \approx 0$
9	If $Vx > 0$ and $Vy > 0$,	then $Vx > 0$

Table 7. Fuzzy rules for the change of V_x in order to improve the operability of the OM

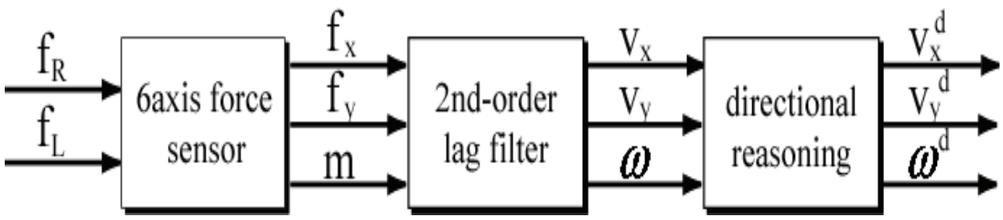

Fig. 37. Block diagram of the power assist system.

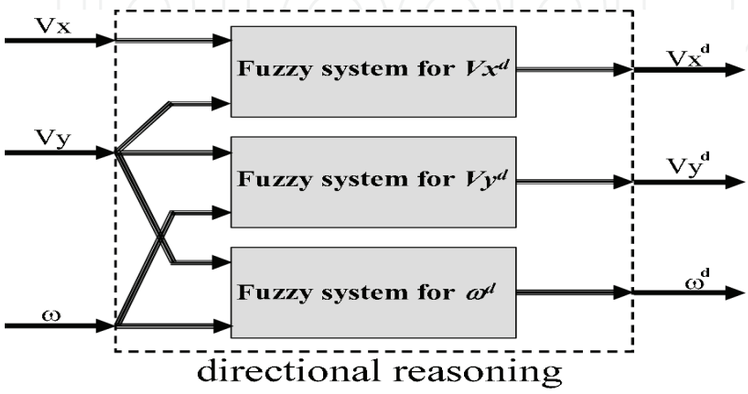

Fig. 38. Contents of the block "directional reasoning".

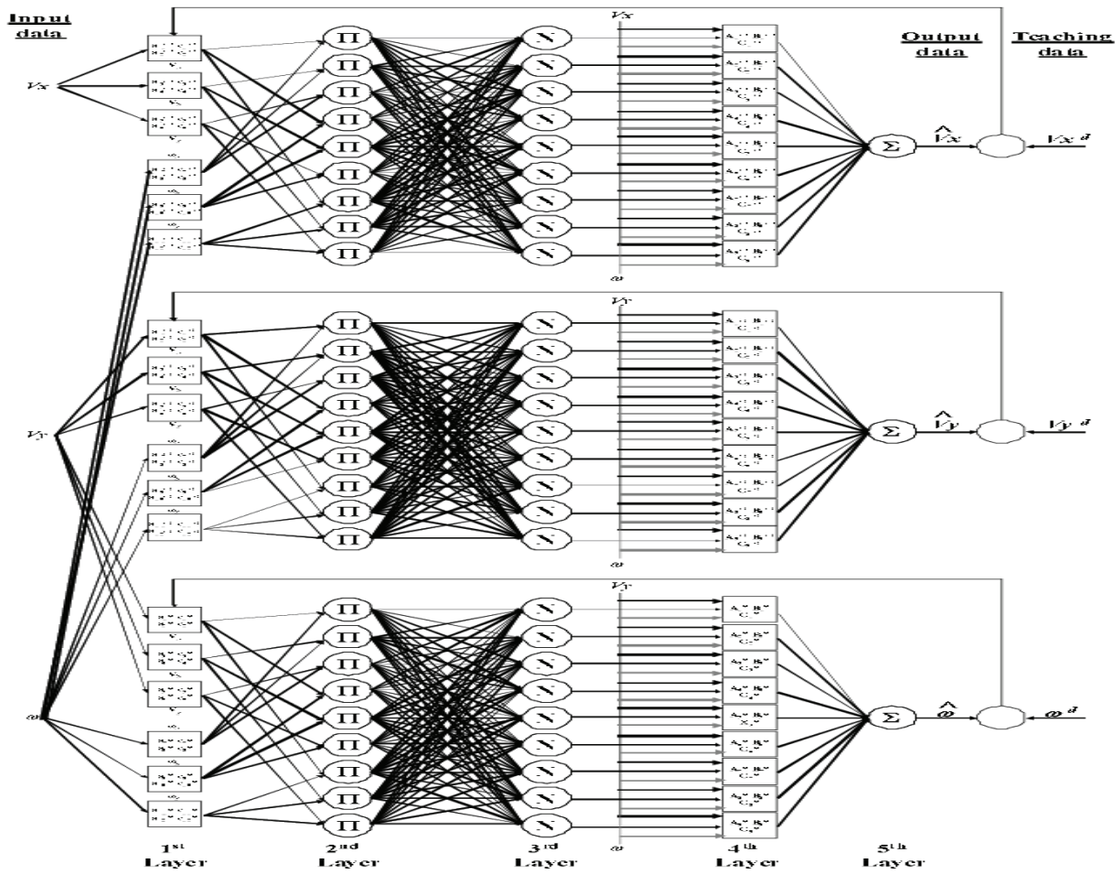

Fig. 39. ANFIS systems of the OMW.

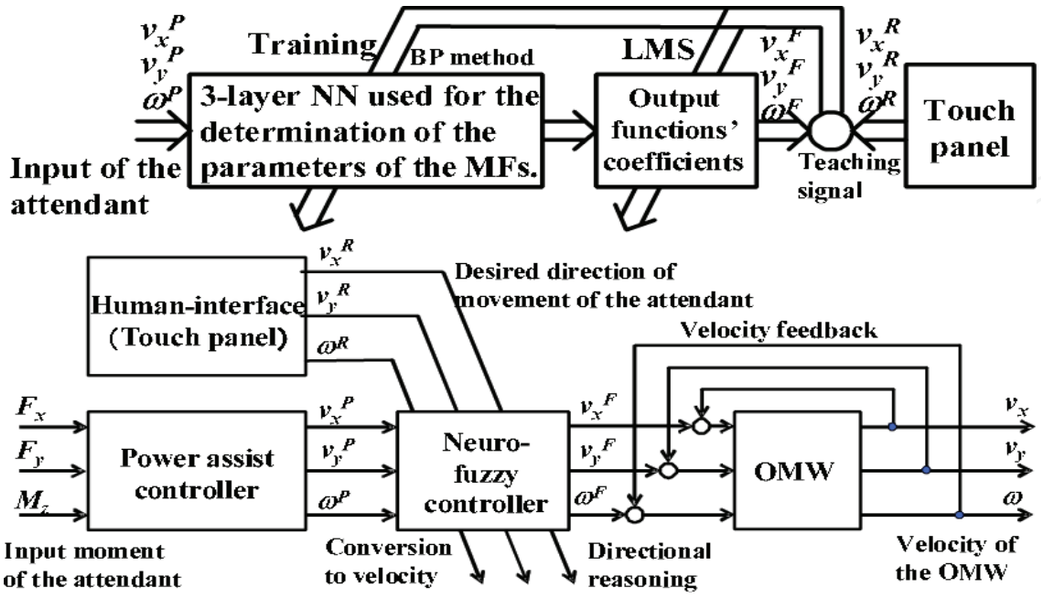

Fig. 40. Complete system when the touch panel is included.

Rule	Antecedents	Consequents
1	**If** Vy_N **and** ω_N,	**then** rotational movement in CW direction
2	**If** Vy_Z **and** ω_N,	**then** rotational movement in CW direction
3	**If** Vy_P **and** ω_N,	**then** lateral movement to the right
4	**If** Vy_N **and** ω_Z,	**then** lateral movement to the left
5	**If** Vy_Z **and** ω_Z,	**then** no movement
6	**If** Vy_P **and** ω_Z,	**then** lateral movement to the right
7	**If** Vy_N **and** ω_P,	**then** lateral movement to the left
8	**If** Vy_Z **and** ω_P,	**then** rotational movement in CCW direction
9	**If** Vy_P **and** ω_P,	**then** rotational movement in CCW direction

Table 8. Fuzzy rules for improving the operability of the OMW

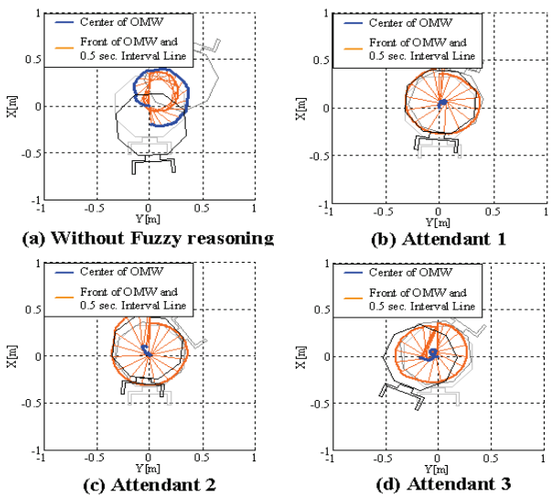

Fig. 41. Results when fuzzy reasoning is not used and when the fuzzy system is tested with different attendants.

As the OMW is so heavy for being easily moved by the attendants, a power assist system has been attached to the OMW in order to help the attendants. However, when the power assist system is attached to the OMW, problems of operability appear, especially in the case of rotation over the center of gravity of the OMW. According to the dynamics of the power assisted system, and the analysis of the data of many attendants, it was possible to determine some rules that the attendants follow when they try to move the OMW in lateral direction, or rotate over the center of gravity of the OMW in counter-clockwise or clockwise direction. These rules are summarized in Table 8, in the form of the fuzzy rules of a fuzzy reasoning system. In Table 8, Vy represents the lateral velocity of the OMW, ω represents the rotational velocity of the OMW and the sub-indices N, Z and P means *negative*, *zero* and *positive*, respectively. Fig. 41 (a) shows the results in the case of a counter-clockwise rotational over the center of gravity of the OMW when no fuzzy reasoning is used. It is possible to see that there is a deviation in the lateral direction as well as in the forwards-backwards direction. For solving this problem, the fuzzy system was used. It was tuned by

trial and error, for an attendant that will be called "Attendant 1", and the results, presented in Fig. 41 (b) show that the rotational movement was improved considerably. However, when the same system was tested with two more different attendants, called "Attendant 2" and "Attendant 3", the results were not as good as in the case of "Attendant 1", as shown in Fig. 41 (c) and Fig. 41 (d). It means that the system must be tuned in order to respond to the individual characteristics of the different attendants. However, the tuning by trial and error is time
consuming and boring for the attendant. For that reason, the automatic tuning of the system by using a neuro-fuzzy system, ANFIS (Adaptive-Neural Fuzzy Inference System) was proposed and developed as described in (Urbano et al, 2006b).

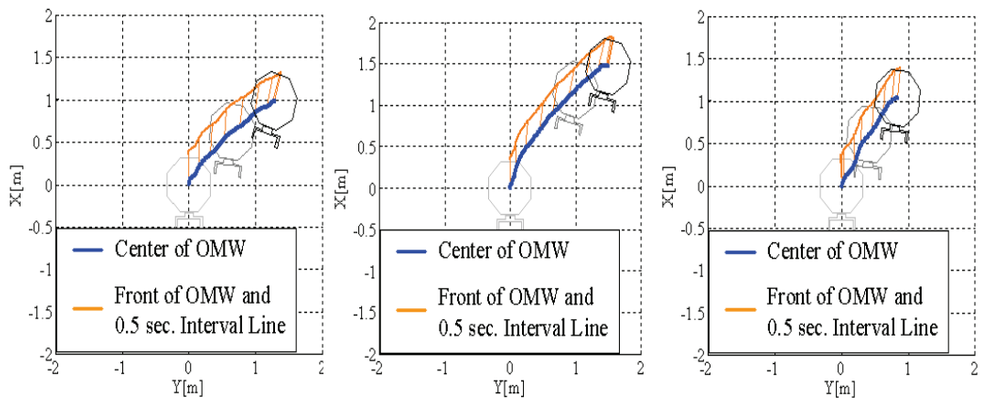

Fig. 42. Experimental results before the tuning of the system.

In previous research (Urbano et al, 2006b), the desired direction of motion of the attendant was inputted by using the keyboard of the computer of the OMW. However, the attendant could not get a clear idea of the direction in which he wanted to move, neither verify if the real motion of the OMW really corresponded to his desire. In order to provide the attendant with an easy way for input of the desired direction of motion and for verifying the direction of motion, a human interface consisting of touch panel, as shown in Fig. 42 is used. A GUI (Graphical User Interface) was developed for making easy the interaction with the attendant. In this GUI the attendant can draw any kind of motion, as for example slanting motion, or a rotational movement. Moreover, it allows the attendant to follow and compare the difference between the desired and the real motion of the OMW. The procedure for applying the touch panel is as follows:

a) First, the attendant draws in the touch panel the kind of movement that he desires to accomplish.

b) Then, the attendant moves the OMW trying to accomplish the desired motion.

c) However, in the general case, there is a difference between the desired motion and the real motion. This difference is used for the training of the ANFIS system of the OMW,

as explained in (Urbano et al, 2005a).

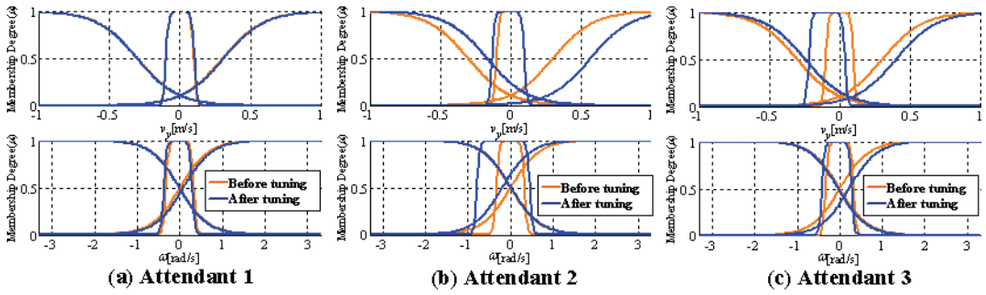

Fig. 43. Variation of the input membership functions of different attendants.

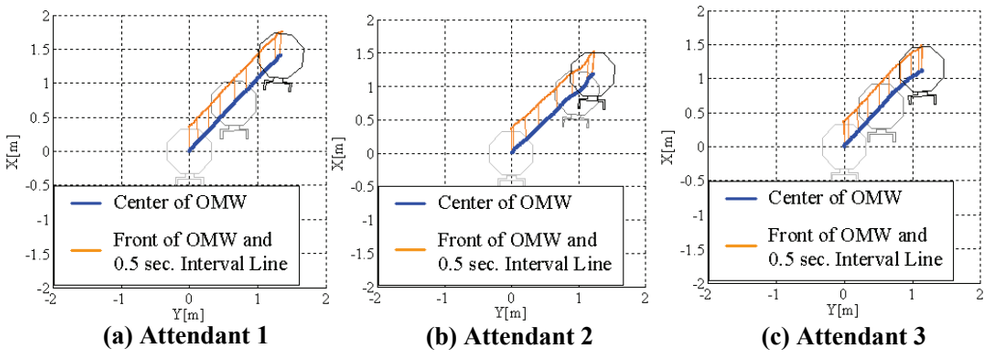

Fig. 44. Experimental results after the tuning of the system

Fig. 42 shows the experimental results for three different attendants before the tuning of the system, and Fig. 44 shows the experimental results for the same three attendants after the system was tuned by using ANFIS. It is possible to see that the movement accomplished by the attendants was greatly improved after the tuning. As shown in the graphs of Fig. 43, the shape of the membership functions of the fuzzy system changes in order to fit to the individual characteristics of each attendant. In the case of "Attendant 1", the membership functions are practically the same before and after the tuning with ANFIS because the system had already being tuned for "Attendant 1". In the case of "Attendant 2", the graphs show that the value of the input of rotational moment and lateral velocity to the right is greater than that of "Attendant 1". Finally, in the case of "Attendant 3" the difference is the width of the null partition of the lateral velocity. These results demonstrate the good performance of the proposed approaches in any case.

6. Comfort Driving of the OMW

The control system is based on a hybrid shape approach recently developed in our laboratory (Yano et al, 2000). Optimization problems formulated in both the time and the frequency domains have scarcely been found in the other researches.
Here, a dynamic model of vibration is not utilized in the control design step, because it

would be difficult to mathematically model the vibrations of the wheelchair and the patient using it. In the design of a controller, the natural frequency of the wheelchair and of the user's organs are utilized as *a priori* information. Controller design is composed of the following elements:

a) Selection of controllers: Controllers are constructed by several fundamental control elements such as a notch filter, low-pass filter, PID elements, and so on.
b) Formulation of design specifications: The design specifications in the frequency and the time domains are expressed by penalty functions.
c) Formulation of an optimization problem: An optimization problem is formulated with constraints expressed by penalty terms.
d) Computation of a controller: The parameters of the controller are computed by solving an optimization problem. In this paper, the Simplex method is applied to solve the problem. Here, the controller is designed in the direction for the first step. In this system, the controller is supposed to be designed in three directions independently, which seems to be achieved easily. In this paper, only X and Y axes will be considered, but not θ axis ($\theta_r = 0$) for brevity. However, consideration of θ is straightforward.

A. Selection of controller

The wheelchair is controlled by a servo system with an integrator. According to the Internal model principle, a proportional control (P control) system is sufficient to avoid the offset. Therefore, a proportional gain is given as an element of this controller.

$$K_1(s) = K_P \tag{39}$$

Two notch filters prevent the controller from exciting vibration in the wheelchair or in the patient's organs, as

$$\mathrm{K}_2(\mathrm{s}) = \frac{\mathrm{s}^2 + 2\zeta\omega_\omega \mathrm{s} + \omega_\omega^2}{\mathrm{s}^2 + \omega_\omega \mathrm{s} + \omega_\omega^2} \tag{40}$$

$$\mathrm{K}_3(\mathrm{s}) = \frac{\mathrm{s}^2 + 2\zeta\omega_0 \mathrm{s} + \omega_0^2}{\mathrm{s}^2 + \omega_0 \mathrm{s} + \omega_0^2} \tag{41}$$

,where the parameters are given as the natural frequency of the wheelchair ω_ω = 15.5 [rad/s] (X-axis) and ω_ω = 15.8 [rad/s] (Y-axis), and that of human's organs ω_0 = 37.7 [rad/s]; and ζ= 0.0001. Since the natural frequencies of the user's organs range from 4 [Hz] to 8 [Hz], the intermediate value is adopted. In order to reduce the influence of higher-order vibration and noise, a low-pass filter, which is the low gain in the high frequency domain, is given as

$$\mathrm{K}_4(\mathrm{s}) = \frac{\omega_l^2}{\mathrm{s}^2 + 2\zeta_l \omega_l s + \omega_l^2} \tag{42}$$

where the parameters are given as $\zeta_l = 0.7$. Finally, the transfer function of the controller is given as

$$K(s) = \prod_{i=1}^{4} K_i(s) = \frac{(K_P \omega_l^2)(s^2 + 2\zeta\omega_\omega s + \omega_\omega^2)(s^2 + 2\zeta\omega_0 s + \omega_0^2)}{(s^2 + 2\zeta_l \omega_l s + \omega_l^2)(s^2 + \omega_\omega s + \omega_\omega^2)(s^2 + \omega_0 s + \omega_0^2)} \tag{43}$$

In this equation, K_P and ω_l are unknown parameters. Therefore, both parameters should reasonably be determined by solving an optimization problem.

B. Formulation of design specifications

The specifications of the controller are formulated by making use of penalty function. Penalties are given if any of the following relations do not hold.

- The controller and the closed-loop system are stable.

$$\mathrm{Re}[r_K] < 0, \quad \mathrm{Re}[r_{cl}] < 0 \tag{44}$$

$$K_P > 0, \quad \omega_l > 0 \tag{45}$$

- The controller gain is less than -20[dB] at the natural frequency of the wheelchair ω_ω = 15.5 [rad/s] (X-axis) and ω_ω = 15.8 [rad/s] (Y-axis),or at that of user's organs ω_0 = 37.7[rad/s].
-

$$\left|K(\omega_w)\right| < -20[dB] \tag{46}$$

$$\left|K(\omega_0)\right| < -20[dB] \tag{47}$$

- The controller gain is less than 0[dB] at ω_l = 188 [rad/s] in order to decrease the influence of the higher-order vibration and noise.

$$\left|K(\omega_l)\right| < 0[dB] \tag{48}$$

- The input voltage u does not exceed a magnitude of 24 [V].

$$\max|u| < 24[V] \tag{49}$$

- Maximum overshoot does not exceed a magnitude of 0.001 [m].

$$\max(O_s) < 0.001[m] \tag{50}$$

C. Formulation of an optimization problem

The following optimization problem using penalty terms is formulated with Eqs. (41) to (47).

$$\min_{K(s)} J = T_s + J_P \tag{51}$$

where

$$J_P = \omega_1 + \omega_2 + \cdots + \omega_9 \tag{52}$$

, and T_s is the settling time when the target position is 2.0 [m] and the admissible error is 0.001[m]. If any of the above penalty conditions are not satisfied, the penalty function w_i is given as $w_i = 10^8 (i = 1,\ldots, 9)$.

D. Computation of a controller

For the optimization of a cost function, the Simplex method is used, where the reflection coefficient α =1.0, the expansion coefficient β =0.5 and the contraction coefficient γ = 2.0. The initial simplex is described in Table 9. As the results of computation, optimum values of K_P and ω_l are shown in Table 10, which was calculated by about 20 times repetition.

	1	2	3
K_P	15	20	30
ω_l	30	40	50

Table 9. Initial simplex

	X-axis	Y-axis
K_P	15.6827	14.6374
ω_l	13.4135	31.6110

Table 10. Results of optimization

E. Control Simulation

By means of Eq. (43) using the values of Table 10, control simulations were done. Trapezoidal reference trajectory was given as x_r. Figures 45 and 46 were respectively simulation results of X-axis and Y-axis. In Fig. 45 and 46, the dotted line and solid line show the case of Feedforward (FF) inputs given by trapezoidal form and hybrid shape approach (HSA) respectively. HSA approached realized the good result without residual vibration in both of X and Y-direction. The frequency response of the controller is shown in Fig. 45. It can be seen that the high-speed transfer is achieved because the controller is high-gain in the

low-frequency domain. The simulation result of the trajectory tracking is shown in Fig. 45 and Fig 46. As seen from this figure, it is confirmed that overshoot is not found.

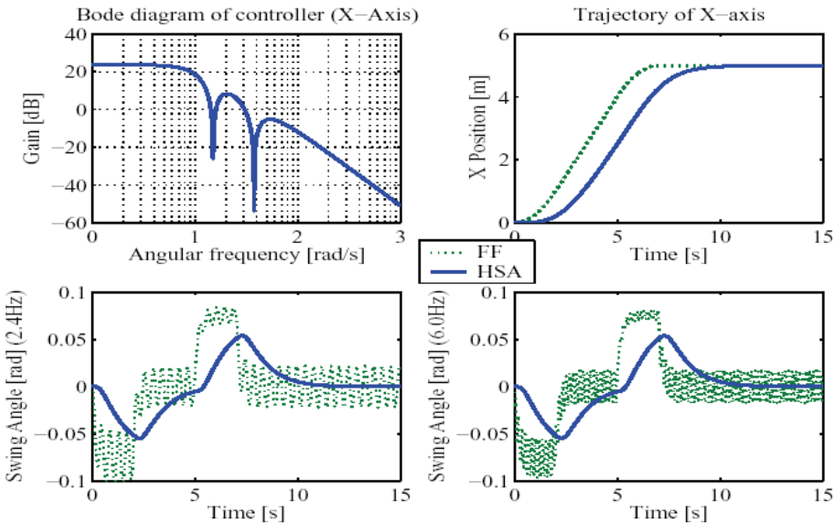

Fig. 45. Simulation results of X-axis

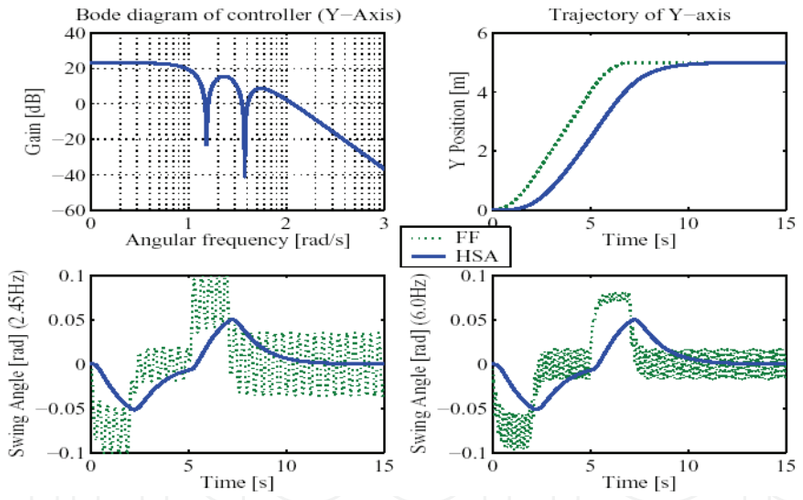

Fig. 46. Simulation results of Y-axis

In order to verify the effectiveness of the control system, laboratory experiments are conducted. In these experiments, the wheelchair moves forward 3.3 [m] (+X direction) and halts three times, for 10 [s] at a time. Two kinds of controllers are examined.

- PD feedback controller without filter
- Proposed controller designed by the hybrid shape approach.

The experimental trajectory is shown in Fig. 47. The experimental results are evaluated by the following two steps. In the first step, the output signal of the acceleration sensor attached to the wheelchair is examined to evaluate the vibration suppression. However, the effectiveness of the consideration of the patient's organs cannot be evaluated in this step. In the second step, the effectiveness of the proposed method on comfort is evaluated by the SD (Semantic Differential), which is a kind of inspection using a scale of verbal. The output of the acceleration sensor attached beneath the seat is shown in Fig. 48. The resultant acceleration and the jerk are suppressed by the hybrid shape approach.

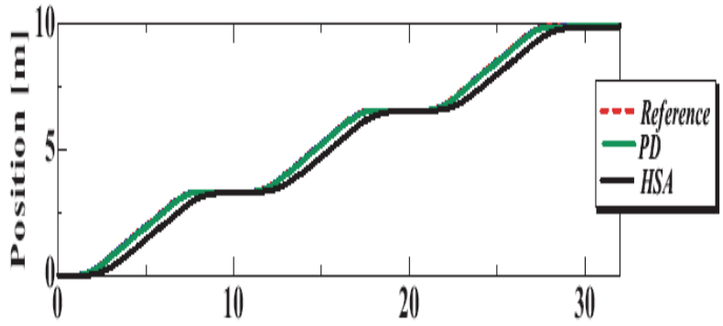

Fig. 47. Trajectory of movement of X-axis

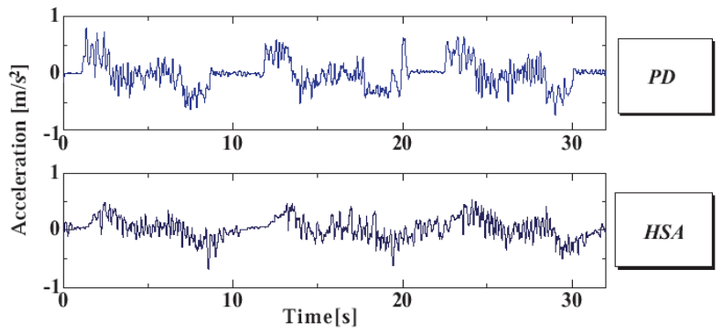

Fig. 48. Experimental results (X-direction)

The SD method is applied to evaluate the effectiveness of the consideration of the patient's organs. In this method, several pairs of adjectives are adopted to evaluate an object or feeling. Within each pair, the adjectives are antonymous each other. To describe the feeling that he or she is experiencing, the examinee selects one of seven grades that form a scale ranging from the one adjective to the other. This method is especially effective for finding the shades of differences among several objects or feelings. The wheelchair was evaluated by 15 examinees. The average value of each item is shown in Fig. 49. The hybrid shape approach seems to enable examinees to provide the greatest sense of patient comfort. Furthermore, Fig. 50 and Fig. 51 are experimental results of Y-direction. The result by HSA

is better than the conventional trapezoidal velocity curve, or, PD controller. Figure 52 shows the experimental results of diagonal direction ($x_r = y_r$, $\theta_r = 0$). In the diagonal movement of OMW, OMW can be transferred comfortably by using the smooth acceleration curve of the proposed HSA. Through this research, it was clarified that vibration suppression and comfort riding in OMW were realized by using the proposed HSA control.

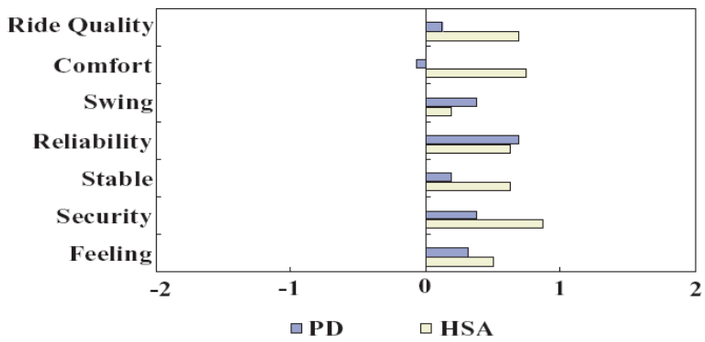

Fig. 49. Result of questionnaire (X-direction)

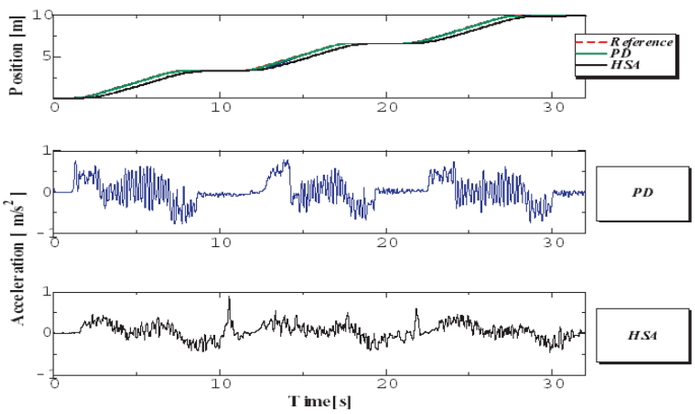

Fig. 50. Experimental Results (Y-direction)

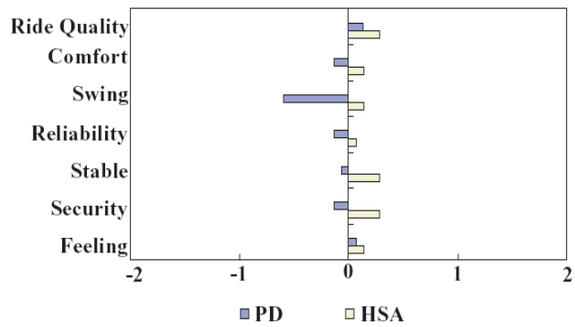

Fig. 51. Results of questionnaire (Y-direction)

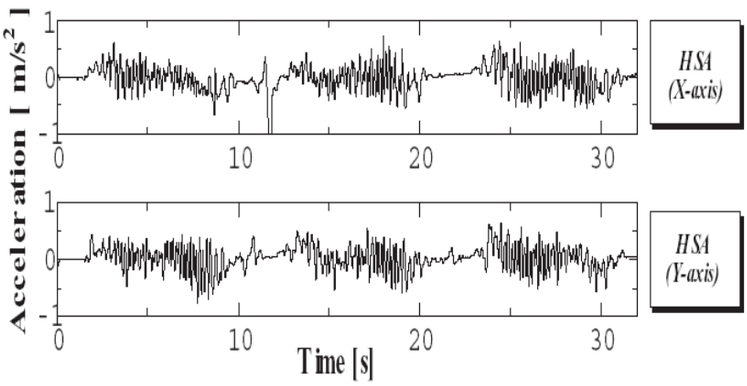

Fig. 52. Experimental result ($x_r = y_r$; $\theta r = 0$)

7. Conclusions

1. A local map was built around the OMW by using range sensors. This local map allows knowing the distance from the OMW to the surrounding obstacles in a circle with a radius of 3 [m].
2. The information provided by the local map, as well as the information of velocity of the OMW were used for varying the stiffness of a haptic joystick that sents information to the hand of the occupant of the OMW. As the distance to the nearer obstacles decreases and the velocity of the OMW increases, the stiffness of the haptic joystick increases, and vice versa. By using the haptic joystick, the occupant of the OMW was able of achieving safety navigation by avoiding collision against obstacles. The sensing system to obtain the surrounding environmental information for any arbitrary direction in real time was built. The algorithm to choose only environmental information existing toward the moving direction of OMW for navigation support system was proposed. Using the constructed environmental recognition system, operation assistance system that informs the danger level of collision to the operator was given. Navigation guidance haptic feedback system that induces an evasive movement to navigate OMW toward the direction without obstacle was proposed.
3. A power assist system was attached to the rear part of the OMW in order to provide support to the attendants of the OMW, specially in the case when the attendant of the OMW is a senior citizen. The operability of the OMW with power assistance was improved by using fuzzy reasoning, but it was found that the membership functions of the fuzzy reasoning system had to be tuned in order to respond to the individual characteristics of each attendant. A neuro-fuzzy system (ANFIS) was used for speeding the tuning of the fuzzy reasoning system of the OMW by using the input data of the attendants. A touch panel with display was attached to the rear part of the OMW for providing a human-friendly interface for the input of the teaching data of the neuro-fuzzy system. Moreover, this touch panel can be used by the attendant for knowing the difference between the desired motion and the real motion of the OMW, and then adjust his behavior according to his observation. The operability of the OMW was improved by using the combined system ANFIS-touch panel.
4. The natural frequencies of the OMW and the natural frequencies of the head and torso

of the occupant of the OMW were suppressed by using the Hybrid Shape Approach (HSA). A human model that considers just the head and the torso of the human being was developed for evaluating the results obtained when the HSA was used. It was found that it was possible to reduce the vibration of the head and torso of the occupant of the OMW by using the HSA.

8. Acknowledgment

We would like to sincerely acknowledge Dr. Y. Noda, Toyohashi University of Technology, and Mr. T. Beppu, T. Kobayashi, T. Nishigaki, Y. Yang and Y.Kondo for author's past graduate students who have collaborated under the supervision of Prof. K. Terashima.
This work was supported in part by COE Program "Intelligent Human Sensing" and furthermore, Global COE Program "Frontiers of Intelligent Sensing" from the Ministry of Education, Culture, Sports, Science and Technology, Japan.

8. References

Ae, M. et al (1992), Estimation of Inertia Properties of the Body Segments in Japanese Athletes, *Journal of Bio-mechanism*, Vol. 11, pp. 23-33

Alsuwaiyan, A. S. & Shaw, S. W. (1999), Localization of Free Vibration Modes in Systems of Nearly-Identical Vibration Absorbers, *Journal of Sound and Vibration*, Vol. 228, No. 3, pp. 703-711

Argyros, A. et al (2002), Semi-autonomous Navigation of a Robotic Wheelchair, *Journal of Intelligent and Robotic Systems,* Vol. 32, pp. 315- 329.

Borgolte, U. et al (1998), Architectural Concepts of a Semi-autonomous Wheelchair, *Journal of Intelligent and Robotic Systems*, Vol. 22, pp. 233-253.

Esen, H. et al (2004), A Virtual Environment Medical Training System For Bone Drilling with 3 DOF Force Feedback, *Proceedings of the 2004 IEEE/RSJ International Conference on Intelligent Robot and Systems (IROS)*, pp. 3631-3636

Funakoshi, M. et al (2004), Measurement of Whole Body Vibration in Taxi Drivers, *Journal of Occupational Health*, Vol. 46, pp. 119-124.

Furusho, H.; Yokoya, K. & Fujiki, S. (1969), Analysis of Occupant's Movements in Head-on Collision (Part1), *Journal of the Society of Automotive Engineering of Japan*, Vol.23, No.10, pp. 1046-1054.

Gen, M. & Cheng, R. (2000), *Genetic Algorithms and Engineering Optimization*, Wiley Series in Engineering Design and Automation.

Goldstein, B. A., et al. (2005), Tinnitus Improvement with Ultra-High-Frequency Vibration Therapy, *International Tinnitus Journal*, Vol. 11, No. 1, pp. 14-22.

Griffin, M. J. (2001), The Validation of Biodynamic Models, *Clinical Biomechanics*, Vol.16 Supplement No. 1, pp. S81-S92.

Hanson, L.; Wienholt, W. & Sperling, L. (2003), A Control Handling Comfort Model Based on Fuzzy Logics, *International Journal of Industrial Ergonomics*, Vol. 31, pp. 87-100.

Harris, C. J. et al (1993), *Intelligent Control*, World Scientific.

Hayashibara, Y. et al (1999), Assist System for Carrying a Long Object with a Human-Analysis of a Human Cooperative Behavior in the Vertical Direction, *Proceedings of the 1999 IEEE/RSJ International Conference on Intelligent Robots and Systems*, pp. 695-

700,.

Holve, R. et al (1995), Generating Fuzzy Rules for the Acceleration Control of an Adaptive Cruise Control System, *Proceedings of the NAFIPS Conference*

Hogan, N. (1985a), Impedance Control: An approach to Manipulation: Part I - Theory, *Journal of Dynamic Systems, Measurement and Control*, Vol. 107, No. 1, pp. 1-7.

Hogan, N. (1985b), Impedance Control: An approach to Manipulation: Part II - Implementation, *Journal of Dynamic Systems, Measurement and Control*, Vol. 107, No. 1, pp. 8-16.

Hogan, N. (1985c), Impedance Control: An approach to Manipulation: Part III - *Journal of Dynamic Systems, Measurement and Control*, Vol. 107, No. 1, pp. 17-24

Jang, J. (1993), ANFIS: Adaptive-Network-Based Fuzzy Inference System, *IEEE Transactions on Systems, Man, and Cybernetics*, Vol. 23, No. 3, pp. 665-685.

Jang, J. et al. (1997), *Neuro-Fuzzy and Soft Computing*, Prentice Hall.

Juang, C. F. and Lin, C. T. (1998), An On-Line Self-Constructing Neural Fuzzy Inference Network and Its Applications, *IEEE Transactions on Fuzzy Systems*, Vol. 6, No. 1, pp. 12-32.

Kaneko, C., et al (2005), Evaluation of Whole-Body Vibration by the Category Judgment Method, *Industrial Health 2005*, Vol. 43, pp. 221-232.

Kaneko, C. et al. (2005), Scaling and Evaluation of Whole-Body Vibration by the Category Judgment Method, *Yamaha Motor Technical Review*.

Kawai, S. et al. (2004), A Study For Control of a Power Assist Device, *Proceedings of the 2004 IEEE/RSJ International Conference on Intelligent Robots and Systems*, pp. 2283-2288

Kitagawa, H.; Kobayashi, T.; Beppu, T. & Terashima, K. (2001), Semi-Autonomous Obstacle Avoidance of Omni-directional Wheelchair by Joystick Impedance Control, *Proc. IEEE/RSJ Int. Symposium on Intelligent Robots and Systems*, pp. 2148-2153

Kitagawa, H.; Beppu, T; Kobayashi, T & Terashima, K. (2002), Motion Control of Omni-directional Wheelchair Considering Patient Comfort, *Proceedings of the IFAC World Congress*, T-Tu-E20

Kitagawa, H.; Nishigaki, T.; Miyoshi, T. & Terashima, K. (2004a), Fuzzy Power Assist Control System for Omni-directional Transport Wheelchair, *Proc. IEEE/RSJ Int. Conf. on Intelligent Robots and Systems*, pp.1580-1585

Kitagawa, H.; Beppu, T; Ohno, Y.; Miyoshi, T. & Terashima, K. (2004b), Motion Control of Omni-directional Wheelchair Considering User's Comfort, *Journal of the Robotics Society of Japan*, Vol.22, No.7, pp.933-939

Kitagawa, H.; Nishisaka, S.; Miyoshi, T & Terashima, K. (2005), Development of Power Assist System for Omni-directional Transport Wheelchair, *Journal of the Robotics Society of Japan*, Vol.23, No.3, pp.321-329

Miyoshi, T. & Terashima, K., (2004), Fuzzy Power Assist Control System for Omni-directional Transport Wheelchair, *IEEE/RSJ International Conference on Intelligent Robots and Systems*pp. 1580-1585

Kondo, Y.; Miyoshi, T.; Terashima, K. & Kitagawa, H. (2008), Navigation Guidance Control Using Haptic Feedback for Obstacle Avoidance of Omni-directional Wheelchair, *Proceedings of Symposium on Haptic Interfaces for Virtual Environments and Teleoperator Systems 2008*, pp. 437-444

Kubo, M. et al (2001), An investigation into a synthetic vibration model for humans: An investigation into a mechanical vibration human model constructed according to

the relations between the physical, psychological and physiological reactions of humans exposed to vibration, *International Journal of Industrial Ergonomics*, Vol. 27, pp. 219-232.

Kumar, V. et al. (1997), *Assistive Devices for People with Motor Disabilities*, Wiley Encyclopedia of Electrical and Electronics Engineering.

Lee, H. et al (1999), Control of Mobile Manipulators for Power Assist Systems, *Proceedings of the 1999 IEEE International Conference on Systems, Man, and Cybernetics*, pp. 989-994

Levine, S. et al (1999), The NavChair Assistive Wheelchair Navigation System, *IEEE Transactions on Rehabilitation Engineering*, Vol. 7, pp. 443 - 451.

Lewis, C. & Griffin, M. (2002), Evaluating the Vibration Isolation of Soft Seat Cushions Using an Active Anthropodynamic Dummy, *Journal of Sound and Vibration*, Vol. 253, No. 1, pp. 295-311.

Lian, T. et al (1999), Tuning of a Neuro-Fuzzy Controller by Genetic Algorithm, IEEE Transactions on Systems, Man and Cybernetics - Part B: Cybernetics, Vol. 29, No. 2, pp. 227-236.

Lin, C. T. & George Lee (1991), C. S., Neural-Network-Based Fuzzy Logic Control and Decision System, *IEEE Transactions on Computers*, Vol. 40, No. 12, pp. 1321-1336.

MathWorks (2002), *Fuzzy Logic Toolbox User's Guide Version 2*, The Mathworks Inc.

Maeda, H. et al (2000), Development of Omni-Directional Cart with Power Assist System (in Japanese), *Proceedings of the 18th Annual Conference of the Robotics Society of Japan*, pp.1155-1156.

Mamdani, E. H. & Assilian, S. (1985), An experiment in linguistic synthesis with a fuzzy logic controller, *International Journal of Man-Machine Studies*, Vol. 7, No. 1, pp. 1-13.

Matsumoto, Y. & Griffin, M. J. (2001), Modeling the Dynamic Mechanisms Associated with the Principal Resonance of the Seated Human Body, *Clinical Biomechanics* , Vol. 16, No. 1, pp. S31-S44.

Matsuoka, Y. (2000a), Vibration Simulation Model for the Transportation of Wheelchair-bound Passengers, *KANSEI Engineering International*, pp. 47-52.

Matsuoka, Y. (2000b), Vibration Evaluation Model on the Wheelchair Transporting Apparatus, *KANSEI Engineering International*, pp. 52-60.

Naruse, K. et al (2005), Three-dimensional Lifting-up Motion Analysis for Wearable Power Assist Device of Lower Back Support, *Proceedings of the 2005 IEEE/RSJ International Conference on Intelligent Robots and Systems*, pp. 3126-3131, (2005).

Nguyen, H. T. et al (2003), *First Course in Fuzzy and Neural Control*, Chapman & Hall CRC.

Nishiyama, S. (1993), Development of Simulation System Vehicle-occupant Dynamic Interaction (in Japanese), *Japanese Society of Mechanical Engineering*, Vol. 59, No. 568) pp. C, 9.

Okada, A. (1980), Sense of Vibration of Man, *Journal of Society of Automotive Engineers of Japan*, Vol. 34, No. 5, pp. 440-450.

Paddan, G. S. & Griffin, M. J. (2000), Transmission of Yaw Seat Vibration to the Head, *Journal of Sound and Vibration*, Vol. 229 No. 5, pp. 1077-1095.

Paddan, G. S. & Griffin, M. J. (2002), Evaluation of Whole-Body Vibration in Vehicles, *Journal of Sound and Vibration*, Vol. 253, No. 1, pp. 195-213.

Parsons, K. C. (2000), Environmental Ergonomics: A Review of Principles, Methods and Models, *Applied Ergonomics*, Vol. 31, pp. 581-594.

Park, S. et al (2001), Single-mode Vibration Suppression for a Beam-Mass-Cart System Using

Input Pre-shaping with a Robust Internal Loop Compensator, *Journal of Sound and Vibration*, Vol. 241, No. 4, pp. 693-716.

Pin, F. & Killough, S. (1994), A new family of omni-directional and holonomic wheeled platforms for mobile robots, *IEEE Transactions on Robotics and Automation*, Vol. 10, No. 4, pp. 480-489.

Protho, J. et al (2000), An Evaluation of an Obstacle Avoidance Force Feedback Joystick, *Proceedings of the Annual RESNA Conference*, Florida, pp. 447-449

Qiu, Y. & Griffin, M. J. (2004), Transmission of Vibration to the Backrest of a Car Seat Evaluated with Multi-input Models, *Journal of Sound and Vibration*, Vol. 288, pp. 297-321.

Qiu, Y. & Griffin, M. J. (2005), Transmission of Roll, Pitch and Yaw vibration to the Backrest of a Seat Supported on a Non-rigid Car Floor, *Journal of Sound and Vibration*, Vol. 274, pp. 1197-1222.

Sanada, K. et al (2005), A Study on Design and Evaluation of a Power-assisted Chair, *Proceedings of the SICE Annual Conference 2005*, pp. 3074-3078

Sato, R.; Iwahashi, Y. & Matsuoka, Y. (2003), Vibration Absorber of Wheelchair Transporting Apparatus and its Effectiveness on Riding Comfort, *The Science of Design*, Vol.50, No.1, pp. 11-18.

Seki, H. et al (2005), Novel Driving Control of Power Assisted Wheelchair Based on Minimum Jerk Trajectory, *IEEJ Transactions on Electronics, Information and Systems*(in Japanese), Vol. 125-C, No. 7, pp. 1133 - 1139.

Shaw, I. S. (1998), *Fuzzy control of industrial systems : theory and applications*, Kluwer Academic Publishers.

Stearns, S. (2003), *Digital Signal Processing*, CRC Press.

Smith, S. (2000), Modeling Differences in the Vibration Response Characteristics of the Human Body, *Journal of Biomechanics*, Vol. 33, pp. 1513-1516.

Sue, J. et al (2006), An Automatic Travel Control of a Container Crane using Neural Network Predictive PID Control Technique, *International Journal of Precision Engineering and Manufacturing*, Vol. 7, No. 1, pp. 35-41.

Sugeno, M. & Kang, G. T (1998), Structure identification of fuzzy model, *Fuzzy Sets and Systems*, Vol. 28, No. 1, pp. 15-33.

Tahboub, K. (2001), A Semi-Autonomous Reactive Control Architecture, *Journal of Intelligent and Robotic Systems*, Vol. 32, pp. 445- 459.

Takagi, T. & Sugeno, M. (1985), Fuzzy Identification of Systems and Its Applications to Modeling and Control, *IEEE Transactions on Systems, Man and Cybernetics*, Vol. 15, No. 1, pp. 116 - 132.

Terashima, K.; Kitagawa H., Miyoshi, T. & Urbano, J. (2004), Frequency Shape Control of Omni-directional Wheelchair to Increase User's Comfort, *Proceedings of the 2004 IEEE International Conference on Robotics and Automation (ICRA)*, pp. 3119-3124.

Terashima, K.; Urbano, J. & Kitagawa, H. (2006), Enhancement of Maneuverability of a Power Assist Omni-directional Wheelchair by Application of Neuro-Fuzzy Control, *Proceedings of the 3rd International Conference on Informatics in Control Robotics and Automation (ICINCO 2006)*, pp. 67-75.

Trampe, J. (1990), *Principles of Experimental Frequency Analysis*, Elsevier Applied Science.

The Japanese Standards Association, (JSA), (2000), *Evaluation of the whole body vibration: TR Z 0006* (in Japanese), The Japanese Industry Standard Committee Basic Sectional

Meeting.

Ueberle, M. & Buss, M. (2002), Design, Control, and Evaluation of a New 6 DOF Haptic Device, *Proceedings of the 2002 IEEE/RSJ International Conference on Intelligent Robot and Systems (IROS)*, pp. 2949-2954, (2002).

Urbano, J.; Terashima, K.; Miyoshi, T & Kitagawa, H., (2005a), Collision Avoidance in an Omni-directional Wheelchair by using Haptic Feedback, *WSEAS Transactions on Systems*, Vol. 4, No. 1, pp. 79-84.

Urbano, J. ; Yang, Y.; Terashima, K.; Miyoshi, T. & Kitagawa, H., (2005b), Navigation with Comfort of Omni-directional Wheelchair Driven by Joystick, *Proceedings of the IFAC World Congress*, Tu-M04-TP/14, (2005).

Urbano, J.; Terashima, K.; Nishigaki, T.; Miyoshi, T. & Kitagawa, H., (2005c), Development of Power Assist on Omni-directional Mobile Wheelchair Considering Operability and Comfort, *Proceedings of the 2nd International Conference on Informatics in Control Robotics and Automation (ICINCO 2005)*, (2005).

Urbano, J.; Terashima, K. & Kitagawa, H., (2006a), Neuro-Fuzzy Control of a Power Assist Omni-directional Wheelchair to Enhance Maneuverability, *Proceedings of the IEEE International Conference on Control Applications (CCA)*, pp. 939-946

Urbano, J. ; Terashima, K. & Kitagawa, H., (2006b), Skill-Assist Control of an Omni-directional Wheelchair by Neuro-Fuzzy Systems Using Attendants' Force Input, *International Journal of Innovative Computing, Information and Control*, Vol. 2, No. 6, pp. 1219-1248.

Wada, M. & Asada, H. (1999), Design and Control of a Variable Footprint Mechanism for Holonomic Omnidirectional Vehicles and its Application to Wheelchairs, *IEEE Transanctions on Robotics and Automation*, Vol. 15, No. 6, pp. 978-989.

West, M. & Asada, H. (1992), Design of a holonomic omni-directional vehicle, *Proceedings of the IEEE International Conference on Robotics and Automation*, pp. 97-103

Wu, Y. et al. (2004), Development of a Power Assisting System of a Walking Chair, *Proceedings of the 2004 IEEE/RSJ International Conference on Intelligent Robots and Systems*, pp. 3207-3212

Yamada, Y. et al (2002), Proposal of Skill-Assist for Mounting Operations in Automobile Assembly Processes, *Transactions of the Japan Society of Mechnical Engineers* (in Japanese), Vol. 68, No. 666, pp. 509-516.

Yanco, H. et al (1995), Initial Report on Wheelesley: A Robotic Wheelchair System, *Proceedings of the Workshop on Developing AI Applications for the Disabled, International Joint Conference on Artificial Intelligence*

Yano, K.; S. Higashikawa & K. Terashima (2000), A Vibration Control Design of Liquid Container Transfer System by Hybrid Shaped Approach Considering the Both of Frequency Characteristics and Time Response, *Proceedings of Movic 2000*, pp. 279-284, Sydney

Yoneda, I. et al (1997), Development of a manual attendant-controlled wheelchair with a foldable plate seat and a mechanism absorbing vibration, *Proceeding of 12th Japanese Conference of Advancement of Rehabilitation Technology*, vol.12, pp. 33-36.

Zhao, X. & Chaffin, D. (2000), A three-dimensional dynamic posture prediction model for simulating in vehicle seated reaching movements: development and validation, *Ergonomics*, Vol. 43, pp.1314-1330.

Frontiers in Robotics, Automation and Control

Edited by Alexander Zemliak

ISBN 978-953-7619-17-6
Hard cover, 450 pages
Publisher InTech
Published online 01, October, 2008
Published in print edition October, 2008

This book includes 23 chapters introducing basic research, advanced developments and applications. The book covers topics such us modeling and practical realization of robotic control for different applications, researching of the problems of stability and robustness, automation in algorithm and program developments with application in speech signal processing and linguistic research, system's applied control, computations, and control theory application in mechanics and electronics.

InTech Europe
University Campus STeP Ri
Slavka Krautzeka 83/A
51000 Rijeka, Croatia
Phone: +385 (51) 770 447
Fax: +385 (51) 686 166
www.intechopen.com

InTech China
Unit 405, Office Block, Hotel Equatorial Shanghai
No.65, Yan An Road (West), Shanghai, 200040, China
中国上海市延安西路65号上海国际贵都大饭店办公楼405单元
Phone: +86-21-62489820
Fax: +86-21-62489821

IntechOpen